Journal of Environmental Radioactivity 298 (2026) 108119

Contents lists available at ScienceDirect

Journal of Environmental Radioactivity

journal homepage: www.elsevier.com/locate/jenvrad

Radiological risk assessment due to naturally occurring radionuclides in water and fish from gold mining-impacted regions in northern Tanzania

Dorice Rashid Seif [a,b], Leja Rovan Stiplošek [b], Mwingereza John Kumwenda [a], Mohamed Mazunga [a], Marko Štrok [b,*]

[a] University of Dar es Salaam, Physics Department, P.O Box 35063, Dar es Salaam, Tanzania
[b] Jožef Stefan Institute, Jamova 39, Ljubljana, SI-1000, Slovenia

ARTICLE INFO

Keywords:
Naturally occurring radionuclides
Drinking water contamination
Radiological risk
Freshwater fish tissues
Age-dependence
Gold mining

ABSTRACT

Many households in gold-mining regions of northern Tanzania have limited access to safe and reliable drinking water and rely on surface water, groundwater, and locally caught fish as key drinking-water and dietary sources, yet the radiological safety of these sources remains uncertain. This study evaluated age-dependent radiological risks from ingestion of naturally occurring radionuclides (^{234}U, ^{238}U, ^{226}Ra, ^{210}Po, ^{210}Pb) in multiple water sources and in fish tissues (bones, gills and flesh) of African lungfish (*Protopterus aethiopicus*), Nile tilapia (*Oreochromis niloticus*) and African Catfish (*Clarias gariepinus*). Activity concentrations were determined by radiochemical separation followed by alpha spectrometry and gas-flow proportional counting. Annual effective dose (AED) and excess lifetime cancer risk (ELCR) were estimated using age-specific water and fish consumption rates. Groundwater, particularly from shallow wells, produced the highest exposures, with a maximum AED for a 5-year-old child, dominated by ^{234}U, exceeding both the World Health Organization (WHO) screening level (0.1 mSv/y) and the International Commission on Radiological Protection (ICRP) public dose reference level (1 mSv/y). Fish consumption was the dominant pathway, with African lungfish consistently yielding the highest AEDs, followed by Tilapia and Catfish. The dose contributions were dominated by ^{210}Pb (75% –96%) and ^{210}Po (4% - 25%), while ^{234}U, ^{238}U, and ^{226}Ra contributed <1%. The estimated ELCRs associated with consumption of all fish species, exceeded the USEPA acceptable risk range ($10^{-6} - 10^{-4}$). Elevated ^{234}U/^{238}U activity ratios (>1) indicated preferential mobilisation of ^{234}U via alpha-recoil, while low ^{210}Po/^{210}Pb ratios (<1) confirmed ^{210}Pb predominance. These findings underscore the need for continued radiological monitoring and targeted mitigation to protect vulnerable communities.

1. Introduction

Naturally occurring radionuclides (NOR) originating from uranium, thorium and actinium decay chains are widespread in the Earth's surface systems, including the lithosphere, biosphere, and pedosphere. These radionuclides are mostly alpha emitters, but many of their short-lived progeny also emit beta and gamma radiations (Hosseini et al., 2008; Srivastava et al., 2013; Štrok et al., 2010a; Wu et al., 2018). Human activities, such as industrial operations, agriculture, and mining, can exacerbate the presence of radionuclides, notably through the release of radioactive elements with mining effluents, thereby contaminating water sources, vegetation, aquatic biota and potentially elevating radiological risks to populations (Ademola et al., 2014; Akoto et al., 2020; El-Taher et al., 2018; Nuccetelli et al., 2012a; Štrok et al., 2010b; Ugbede et al., 2020).

The mobility and transfer of radionuclides in ecosystems are influenced by various factors such as the chemical characteristics of the element, the physicochemical properties of soil or water (such as pH, organic matter content, competing ions, and redox conditions), and the extent of uptake by different types of biota (Botwe et al., 2017; Smodiš et al., 2014). The fate and distribution of radionuclides within aquatic environments are determined by biogeochemical reactions such as dissolution, hydrolysis, complexation, sorption/desorption, and coprecipitation (Nuccetelli et al., 2012a; Štrok and Smodiš, 2011c).

Throughout early human civilization, groundwater and surface water were utilized interchangeably or as substitutes for each other as a source of drinking water and domestic use (Ugbede et al., 2020). Among the diverse sources of water, groundwater remains a significant global

* Corresponding author.
E-mail address: marko.strok@ijs.si (M. Štrok).

https://doi.org/10.1016/j.jenvrad.2026.108119
Received 23 February 2026; Received in revised form 22 July 2026; Accepted 23 July 2026
Available online 28 July 2026

reservoir of safe water for drinking, domestic use, and agricultural and industrial operations (Abed et al., 2021; Chander et al., 2023; Isinkaye et al., 2025; Jakóbczyk-Karpierz et al., 2020). Both groundwater and surface water sources are vulnerable to contamination by natural radionuclides (Akpanowo et al., 2021; Baják et al., 2023; Benedik et al., 2015; Rožmarić et al., 2012a,b). In an aquatic environment, radionuclides such as uranium isotopes (^{234}U and ^{238}U), ^{226}Ra, ^{210}Pb, and ^{210}Po are readily transferred through the aquatic food web, accumulating in fish tissues and subsequently contributing to internal exposure among populations relying on local water and fish resources (Kazoka et al., 2023; Rožmarić et al., 2012; Štrok and Smodiš, 2011a). Ingestion of radionuclides such as U and Ra can result in chemical and radiological toxicity, with associated risks including cancer, organ damage, and genetic effects (Ugbede et al., 2020). For the radiological protection of the public, a screening reference level of 0.1 mSv/y for annual effective dose from drinking water ingestion is recommended by the World Health Organization (World Health Organization, 2011, 2022), and 1 mSv/y is recommended by the International Commission on Radiological Protection (ICRP) for all generated sources of exposure (ICRP, 2007a; ICRP, 2013). Exceeding WHO and ICRP reference levels does not immediately signify an unacceptable health risk but requires further assessment of the acceptability of the risk and, in the case of unacceptable risks, implementation of risk-reduction strategies. As such, exceeding the reference levels helps identify critical exposure pathways and the most affected population groups, and streamline further investigations and monitoring strategies to ensure adequate protection of the population from excessive exposure to ionizing radiation.

Globally, several studies have assessed radionuclide contamination in water and associated aquatic biota, especially where mining activities perturb natural systems (Goulet et al., 2022; Putri et al., 2022; Rovan et al., 2021; Štrok and Smodiš, 2011b; Viloria et al., 2020). The results demonstrated that NOR (^{238}U, ^{226}Ra, ^{228}Ra, ^{210}Pb, ^{210}Po) and other decay products can elevate radiation doses to humans and biota, including freshwater/marine fish and benthic invertebrates. In addition, existing studies in Africa have also documented elevated radionuclides in groundwater near mining areas, with ingestion doses, especially for children, exceeding World Health Organization (WHO) and United Nations Scientific Committee on Effects of Atomic Radiation (UNSCEAR) reference levels, though data regarding radionuclides in aquatic biota, including uptake in fish, still remain scarce (Akpanowo et al., 2021; Bello et al., 2020; Isinkaye et al., 2025).

Large-scale and artisanal gold mining operations are prevalent in Northern Tanzania, particularly in the Mara Region, where local communities depend almost entirely on untreated surface water, shallow wells, boreholes, and fish caught from nearby water bodies for their daily needs, making ingestion the primary route of exposure to NOR. Subsequently, ^{238}U and ^{234}U contribute both chemical and radiological toxicity, while ^{226}Ra and ^{210}Pb tend to accumulate in bones and mineralized tissues. Among the alpha-emitting radionuclides (^{238}U, ^{234}U, ^{226}Ra and ^{210}Pb), ^{210}Po is especially significant because of its strong accumulation in soft tissues such as fish flesh and organs, making it a major contributor to ingestion dose in aquatic consumption (Benedik et al., 2024; Farcas et al., 2020; Friday et al., 1996; Hosseini et al., 2008; Li et al., 2020; Štrok and Smodiš, 2011b).

Based on the studies conducted in Tanzania, radiological assessments in mining environments have been confined mainly to soils, sediments, tailings, or occupational exposure (Focus et al., 2022; Kimaro and Mohammed, 2015), with a limited number of research on radionuclides in water and aquatic biota (Kazoka et al., 2023; Kimaro and Mohammed, 2015; P. Banzi, 2016a), and with little emphasis on: comparative behaviour of radionuclides across multiple water sources (surface water, shallow wells, boreholes), tissue-specific bioaccumulation in fish, seasonal variation, and age-dependent radiological dose and cancer risk assessment associated with water and fish ingestion. The absence of integrated water–fish radioecological studies in Northern Tanzania therefore represents a critical concern. There is a need to assess exposure to radioactivity present in water and fish in the region. A comprehensive evaluation can provide a realistic picture of radiological exposure for households that rely on these local resources in mining-impacted regions. Therefore, in this work, the levels of ^{238}U, ^{234}U, and ^{226}Ra in water (both surface and groundwater) and fish tissues (^{238}U, ^{234}U, ^{226}Ra, ^{210}Pb, ^{210}Po) used by the population residing in the proximities of gold mining areas of Mara Region were determined and annual effective dose, and cancer risk arising from water and fish consumptions was estimated for different age groups.

2. Materials and methods

2.1. Description of study area

The study area is located in Rorya and Tarime Districts within the Mara Region of Tanzania, situated in the North-West of the country between latitudes 1°00′ and 1°45′S and longitudes 33°30′ and 35°00′E (shown in Fig. 1) at elevations ranging from 800 to 1500 m above sea level. The region hosts both active and historical gold mining activities, which have the potential to influence the mobilisation and distribution of naturally occurring radionuclides in the surrounding environment.

The region is characterised by an equatorial hot and humid climate with a bi-modal rainfall pattern (long rains from March to May and short rains from October to December) and temperatures between 14 °C and 30 °C. The region encompasses Rorya District, bordered by Kenya (Migori and Suba counties) to the north, Tarime District to the east, Musoma District to the south, and Kagera Region to the west, with its western margin along the eastern shoreline of Lake Victoria. The regional hydrology is dominated by the Mara River, which originates from the Mau Escarpment in Kenya, flows through the Maasai Mara National Reserve and the Serengeti National Park, and ultimately discharges into Lake Victoria. In addition to the Mara River, the Mori River and its tributaries also drain into Lake Victoria within the study area (Omolo et al., 2018).

Regional geology of the Mara region is diverse, featuring Archean greenstone belts (Nyanzian and Kavirondian Supergroups) with metavolcanic (basalts, andesites, rhyolites) and metasedimentary rocks (banded iron formations, cherts, shales), large granitoid intrusions (granite, granodiorite, tonalite), Proterozoic sedimentary rocks, and Quaternary alluvial deposits. These geological formations host significant mineral deposits, including gold and heavy minerals (Kabete et al., 2012; Kazimoto and Ikingura, 2014). While there is no direct uranium or gold mining downstream of the Mara River Wetland, upstream mining activities, notably gold mining in the nearby Tarime District and in Kenya, can influence the environmental quality of the Mara River through transboundary pollution. Additionally, agricultural runoff and natural geochemical processes may contribute to potential contamination of the river system, impacting water quality and local ecosystems.

2.2. Sampling and sample preparation

2.2.1. Water samples

A total of eighty-nine (89) water samples were collected from rivers (Mara and Mori rivers), streams, boreholes, shallow wells, and dug wells of both privately and government/community-owned sources for drinking and other domestic purposes during the rainy (32 samples) and dry (47 samples) seasons (March and August 2024). At each sampling location, triplicate samples were collected using pre-cleaned, high-density polyethylene (HDPE) bottles to ensure robust field-level replication, which yielded a total of 267 L of water for two seasons. Before groundwater sampling, boreholes were purged to allow water to flow for at least 3 min to ensure that the sample is representative of the groundwater (Benedik et al., 2015). Surface water samples were collected at 0-15 cm below the water surface by submerging uncapped sampling bottles upside down.

The collected water samples were filtered on-site through 0.45 μm

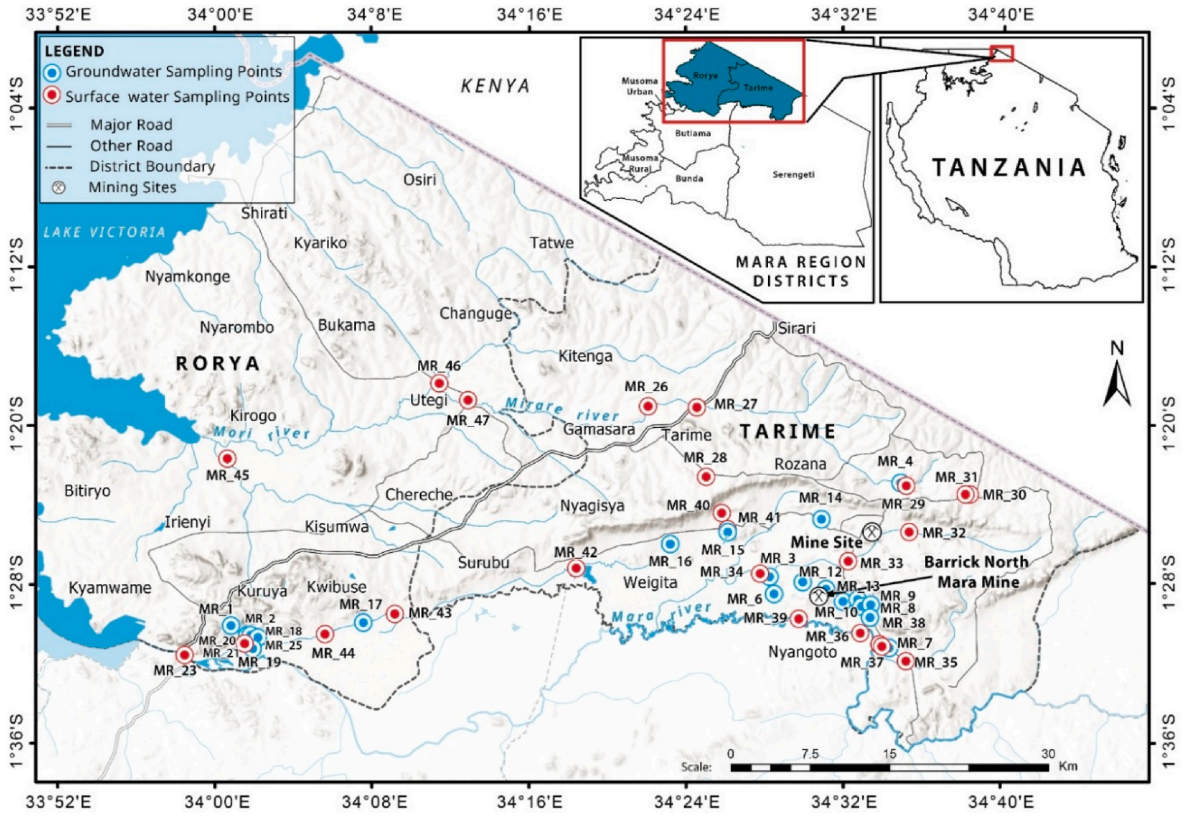

Fig. 1. A map showing sampling locations for ground and surface water along the Mara River, Mori River and Tributaries in northern Tanzania.

pore size filters (Minisart 16555K) and acidified with concentrated supra-pure HNO_3 to pH < 2 to prevent adsorption of radionuclides onto container walls within 12 h after sampling, then stored in 1 L prewashed high-density polyethylene (HDPE) bottles (prewashed using 10% v/v HNO_3 and rinsed several times using deionised water). During sampling, each prewashed sampling bottle was rinsed three times again with surface water (Benedik et al., 2015; Tonev et al., 2023). Sampling locations are presented in Fig. 1, whereas sampling codes, geographical information, and on-site physicochemical parameters (dissolved oxygen (DO), electrical conductivity (EC), turbidity, temperature (T), Total Dissolved Solids (TDS), and Potential Hydrogen (pH)) are presented in Tables S1 and S2. All water samples were shipped to the Jožef Stefan Institute laboratory in Ljubljana, Slovenia, for analysis.

2.2.2. Fish samples

Three fish species (Tilapia, African Lungfish, and Catfish) commonly consumed by local communities were collected from the Mara River at Kirumi and Kukona during the dry season. The species were selected for analysis based on their ecological and feeding behaviour; African Lungfish (*Protopterus aethiopicus*) and Catfish (*Clarias gariepinus*) represent benthic bottom-dwelling taxa that inhabit substrates and feed near sediments (Gartner et al., 2022; Tesfahun and Alebachew, 2023), whereas Tilapia (*Oreochromis niloticus*) is a demersal–benthopelagic species that forages in both mid-water and near-bottom habitats (Temesgen et al., 2022). A total of six samples, each weighing about 2 kg, were collected. Individual fish were subsequently dissected into the following distinct tissue fractions: muscle (flesh), gills, and bone (comprising vertebrae and skull). Each tissue fraction was thoroughly rinsed with deionised water to remove adhering debris and freeze-dried to constant weight for 45 h (Benedik et al., 2024; Putri et al., 2022; Štrok and Smodiš, 2011b). Dried fish tissues were then shipped to the Jožef Stefan Institute laboratory in Slovenia for analysis.

2.3. Analytical procedures

2.3.1. Radiochemical separation of uranium isotopes (^{238}U, ^{235}U, and ^{234}U) in water

Uranium isotopes were determined by alpha spectrometry following radiochemical procedures used to isolate uranium from the matrix, as described by Benedik et al. (2015) and Tonev et al. (2023). To a known volume of water (approximately 0.5 L), a known amount of uranium ^{232}U tracer (~0.03 Bq) was added to the water sample (for quantification and recovery control). Uranium was co-precipitated with iron (III) chloride ($FeCl_3$) at pH 9 – 10, followed by the addition of ammonia solution (NH_4OH). The precipitate was separated from the overlying water by decantation and centrifugation and dissolved in 3 M HNO_3. Uranium was separated by using uranium tetravalent actinide (UTEVA) extraction chromatographic resin, micro-precipitated with Nd^{3+}, followed by the addition of $TiCl_3$ and concentrated hydrofluoric acid (HF). The precipitate was allowed to form at 4 °C for 30 min. The suspension was then filtered through a 25 mm diameter 0.1 μm polypropylene filter, mounted on an aluminium disc, and dried.

2.3.2. Radiochemical separation of ^{226}Ra in water

The analytical procedures for the determination of ^{226}Ra, adapted from (Benedik et al., 2010, 2015), involve the addition of ^{133}Ba tracer to a known volume of water (approximately 0.7 L), followed by co-precipitation of radium and barium (in $Pb(Ra)(Ba)SO_4$) with Pb^{2+} and the addition of concentrated sulphuric acid (H_2SO_4) during stirring. After the precipitate settled to the bottom, the overlying water was decanted, and precipitate was centrifuged; the supernatants were discarded. The $PbSO_4$ precipitate containing radium and barium was dissolved in 4 mL of 0.1 M EDTA/0.5 M NaOH, followed by the addition of 1:1 acetic acid solution until pH 4 – 5 was attained while stirring, thus precipitating $BaSO_4$, while Pb^{2+} ions remained in solution. To the solution, saturated Na_2SO_4 solution and 0.125 mg mL^{-1} $BaSO_4$ suspension

was added, acting as a seeding precipitate to obtain small particles. The precipitate was allowed to form for 30 min, then filtered through a 25 mm-diameter 0.1 μm polypropylene filter. The filter with $Ba(Ra)SO_4$ deposit was dried, mounted on an aluminium disc and then dried again (Benedik et al., 2010).

2.3.3. Digestion procedures for the determination of uranium isotopes and ^{226}Ra in fish tissues

Prior to radionuclide determination, a subsample of about 6 g taken from each fish tissue was ashed at 650 °C in a muffle furnace for 5 h in order to eliminate organic matter. A known mass of the ashed samples in a platinum crucible was then fused together with ^{232}U tracer (0.1 mL), ^{133}Ba tracer (0.6 mL), and 3 g of lithium borates in a Claisse LeNeo furnace at 1050 °C for 23 min. After fusion, the glass was immediately poured into 100 mL of stirred deionised water in a Teflon beaker. The content was then transferred to a glass beaker, stirred, and heated to 125 °C, followed by the addition of 10 mL concentrated HNO_3 to dissolve the obtained glass (lithium borate glass). When the volume of solution was reduced to 50 mL, the temperature was decreased to 90 °C. After the cooling of the sample, 1 mL of 0.2 M polyethylene glycol solution (PEG) was added (to remove silicates), and stirring was applied for 1 h. The solution was left overnight. The sample was filtered before loading on the column through a quantitative filter paper (Nursapina et al., 2022; Štrok et al., 2010c).

2.3.4. Radiochemical separation for simultaneous determination of ^{226}Ra, ^{238}U, ^{235}U, and ^{234}U in fish tissues

Extraction chromatographic separation techniques based on tetravalent actinides (TEVA) and Uranium and tetravalent actinides (UTEVA) resins (Eichrom Technologies) adopted from (Nursapina et al., 2022; Planinšek et al., 2016; Štrok et al., 2010b) were used in the separation of radium and uranium isotopes in the fish tissues. An extraction chromatographic resin UTEVA, was used for the separation of uranium isotopes. A TEVA extraction chromatographic resin was used for the separation of thorium isotopes, while radium isotopes passed through both columns. In more detail, the sample was loaded onto TEVA and UTEVA resins in a column. The columns were first preconditioned by washing with 10 mL of deionised water, 10 mL of 1 M HNO_3, and 10 mL of 3 M HNO_3. The sample was filtered onto a quantitative filter paper when loaded onto the column, and the filter was washed with 5 mL of 3 M HNO_3 prior to removal. 30 mL of 3 M HNO_3 was used to elute Ra from the column. Then the columns were separated, and the UTEVA column was further washed with 5 mL of 9 M HCl and 25 mL of 5 M HCl-0.05 M oxalic acid to remove residual of thorium and other interfering radioisotopes. Then, uranium radioisotopes were washed out with 15 mL of 1 M HCl. After separation processes, alpha-emitting sources were prepared by micro-coprecipitation. Uranium isotopes were micro-coprecipitated with NdF_3, whereas ^{226}Ra was micro-co-precipitated by using $Ba(Ra)SO_4$ as described by Planinšek et al. (2016); Štrok et al. (2010a); Štrok and Smodiš (2011d).

2.3.5. Radiochemical separation procedures for determination of ^{210}Po in fish tissues

To a known mass of the sample (~5 g flesh; ~ 2 g gills/bones) in the Erlenmeyer flask, a known activity of ^{209}Po tracer (0.15 mL) was added for chemical recovery determination of the radiochemical separation. The sample was digested with 25 mL of concentrated HNO_3 and 5 mL of concentrated HCl overnight at room temperature, covered with a watch glass. The sample was heated at 200 °C for 30 min, then cooled. After cooling, 10 mL H_2O_2 was added, and the solution was evaporated to dryness at 100 °C. The procedure was repeated three times. To remove the remaining HNO_3, 2 mL of concentrated HCl was added, and then the mixture was evaporated to incipient dryness.

For the determination of ^{210}Po, the dry digested sample residue was dissolved in 2 mL of concentrated HCl, and diluted to 100 mL deionised water. In order to reduce Fe(III) and prevent coplating of iron and interfering elements, 0.3 g of ascorbic acid was added to the solution. This was followed by the spontaneous deposition of polonium on a 19 mm-diameter silver disk (fixed in a holder, immersed in the solution while covered on one side) at 90 °C for 4 h, while stirred with the stirring bar. After the deposition was finished, the disk was rinsed with deionised water and dried in air (Benedik et al., 2024; Jia et al., 2001; Štrok and Smodiš, 2011b).

2.3.6. Radiochemical separation procedures for determination of ^{210}Pb in fish tissues

For the determination of the recovery of radiochemical separation, to a known amount of sample (~5 g flesh; ~ 2 g gills/bones), a known amount of Pb^{2+} carrier (2 mL) was added. The sample was then digested with 30 mL of concentrated HNO_3 and 6 mL of concentrated HCl overnight at room temperature, covered with a watch glass. The sample was heated at 200 °C for 30 min in a covered Erlenmeyer flask. The solution was then cooled at 100 °C, and the sample was evaporated to dryness. To the residue, 10 mL H_2O_2 was added, and the solution was evaporated to dryness at the same temperature. The remaining precipitate was dissolved with 6 mL HCL and evaporated to dryness at 100 °C. The precipitate was then dissolved with 10 mL of 2 M HCl and filtered through a quantitative filter paper.

Then Pb was separated from other radionuclides using Sr Resin extraction chromatographic resin(Triskem International) according to the procedure described by Štrok and Smodiš (2011b) and Vrecek et al. (2004). To the Sr Resin separation column, which had been conditioned with 50 mL of deionised water, 50 mL of 1 M HCl, and 50 mL of 2 M HCl, the filtrate was introduced. The column was then washed with 50 mL of 2 M HCl, followed by a consecutive addition of 60 mL of 6 M HNO_3. All these eluates were discarded. In a clean beaker, Pb was stripped from the column by adding 60 mL of 6 M HCl, and the solution was evaporated to dryness, then dissolved in 30 mL of deionised water. The sample was then filtered through a quantitative filter paper, 2 mL of concentrated H_2SO_4 was added to precipitate $PbSO_4$ from the solution, the mixture was stirred for 30 min to allow all the $PbSO_4$ to precipitate from the solution, and centrifuged. The supernatant was decanted, and the precipitate was washed with deionised water and centrifuged again. The procedure was repeated until the supernatant reached neutral pH. Then the precipitate was transferred into a specially designed centrifuge tube, which allows a counting planchet to be placed on the bottom, and the tube was centrifuged again. After that, the solution was removed, and the counting planchet with the PbSO4 precipitate was dried under a heating lamp and weighed to determine the radiochemical recovery of the separation gravimetrically. Prepared sources were left for about 30 days to allow for in-growth of ^{210}Bi.

2.4. Measurements

^{238}U, ^{235}U, ^{234}U, ^{226}Ra, and ^{210}Po were measured on an alpha spectrometry system equipped with passivated implanted planar silicon detectors (Alpha Analyst, Canberra), which was calibrated with a mixed alpha certified standard with activity traceable to SI units. Chemical recoveries for uranium were determined by the same system, and those for ^{226}Ra were determined by measuring ^{133}Ba on a gamma-ray spectrometer consisting of a Hyper Pure-Germanium (HP–Ge) detector connected to a multichannel analyser (Spectrum Master 919, Ortec). ^{133}Ba activity was determined relative to a^{133}Ba certified standard solution with activity traceable to SI units, which was evaporated onto an aluminium disc to achieve the same geometry (Benedik et al., 2015; Štrok et al., 2010b). ^{210}Pb was measured on a low-background gas-flow proportional counter, previously calibrated to allow corrections due to in-growth of ^{210}Bi and different self-absorptions for samples with different chemical recovery (Štrok et al., 2008). Chemical recovery for ^{210}Pb was determined gravimetrically by weighing the $PbSO_4$ precipitate. All tracers used were prepared from certified standard radioactive solutions with activities traceable to SI units; blanks were also prepared

and processed using the same radiochemical separation procedure as for the samples.

The minimum detectable activity (MDA) concentration was calculated according to (International Organization for Standardization (ISO), 2025) and depended on detector background, counting time, detector efficiency, chemical recovery, and sample mass. Consequently, the MDA varied among samples rather than being represented by a single value. Typically, alpha spectrometry detection limits achieved were in the range of 1E-4 Bq.

2.5. Health risk assessment due to exposure to NORs in water and fish

2.5.1. Annual effective dose from water ingestion and fish consumption

The annual effective dose (AED) due to ingestion of radionuclides (^{238}U, ^{234}U, and ^{226}Ra) in water was estimated for different age groups (infants, children, and adults), adopted from ICRP Publication 119 (ICRP, 2013), using the activity concentrations of the radionuclides determined in water samples according to Equation (1). Doses were calculated for infant, children, and adult age groups (Table 1) based on the annual water consumption estimated by (UNSCEAR, 2000; World Health Organization (WHO), 2022).

$$AED_{ij} = C_i * IR_j * DCF_{ij} \quad (1)$$

In Equation (1) AED_{ij} represents annual effective ingestion dose due to relevant radionuclide for specific age group in mSvy^{-1}; C_i is the activity concentrations of radionuclide *i* in the water (BqL^{-1}); DCF_{ij} is the dose conversion factor of radionuclides for specific age group (mSvBq^{-1}); and IR_j is the drinking water ingestion rate for age group (Ly^{-1}). Table 1 shows the dose conversion factors (from ICRP, 2013) used in calculating the AED_{ij}. The annual consumption rate of water for the different age groups were extracted from publication by the WHO (World Health Organization, 2011, 2022). The total annual effective dose from water for each age group was obtained by summing the contributions from all radionuclides considered.

To account for seasonal variability in radionuclide concentrations, AED values were first calculated independently for dry and rainy seasons. The total annual effective dose was then estimated by assuming equal exposure durations for both seasons (six months each) according to equation (2):

$$AED = 0.5 * AED_{dry} + 0.5 * AED_{rainy} \quad (2)$$

To ensure comparability, the same dosimetric framework was adopted for fish ingestion of specific radionuclides (^{238}U, ^{234}U, ^{226}Ra, ^{210}Po, and ^{210}Pb) measured in fish tissues (flesh, bones, and gills) as shown in Equation (3):

$$AED_{fish} = C_{dw} * IR_{dw,yr} * DCF \quad (3)$$

Where; $IR_{dw,yr} = IR_{wt,yr} * 0.30$ (assuming 70% of fish is moisture and 30% is dry matter); C_{dw} is the activity concentrations of radionuclide in fish tissue in dry weight (Bq/kg); *DCF* is the dose conversion factor of radionuclides for specific age group (mSvBq^{-1}); and $IR_{dw,yr}$ is the annual fish intake in dry weight based on age group (kg/y), with assumption that each adult eat 0.5 kg fresh weight (f.w) per day ≡ (0.5 kg (f.w) * 365 * 30% of fish moisture) = 54kg/y dry weight; and infants eat 0.125 kg fresh weight (f.w) per day ≡ (0.125 kg (f.w) * 365 * 30% of fish moisture) = 13.7kg/y dry weight; and children eat 0.25 kg f.w per day ≡ (0.25 kg (f.w) * 365 * 30% of fish moisture) = 27.4 kg/y dry weight. Total annual effective dose from fish for each age group was obtained by summing contributions from all radionuclides considered. In the calculation of AED and the percentage contribution of individual radionuclides to the total dose, the mean activity concentrations of the edible fish flesh for each species were used.

2.5.2. Cancer risk assessment

The excess lifetime cancer risk (*ELCR*) due to ingestion of radionuclides or fish based on the age groups was calculated using Equation (4) (ICRP, 2007b; UNSCEAR, 2000). Since the ingestion dose varies with age, ELCR was calculated by summing cancer risk contributions across the respective age intervals up to 70 years, rather than applying a single life expectancy to a single group.

$$ELCR = \sum_i AED_{annual,i} * RF * \Delta t_i \quad (4)$$

Where $AED_{annual,i}$ is the annual effective ingestion dose for age group i (mSv/y), Δt_i is the duration (years) of the corresponding age interval, and *RF* is the risk factor in Sv^{-1}. The risk factor is equal to 5.2×10^{-2} Sv^{-1} according to the nominal probability coefficient recommended by ICRP (2007b).

2.6. Statistical analysis

Seasonal differences of water parameters and activity concentrations of NORs in water sources (surface water, shallow wells, boreholes) were evaluated using Shapiro-Wilk and.

Kolmogorov-Smirnov non-parametric tests due to the typically skewed distribution of radiological data. Due to the skewed distribution of both physicochemical parameters and radionuclide activity concentrations data, the results were presented using median and range (minimum-maximum) instead of the mean. Relationship between radionuclides and basic water quality parameters were assessed using Spearman's rank correlation coefficient. Principal component analysis (PCA) was further applied to identify the dominant geochemical processes and potential seasonal patterns influencing radionuclide distributions. All statistical analyses were performed using Python with significance set at $p < 0.05$.

3. Results and discussion

3.1. Physico-chemical parameters in water

The physicochemical parameters of water (T, pH, EC, TDS, DO, and Turbidity), varied between dry and rainy seasons, as shown in Fig. 2a-f and Tables S1 and S2. Temperature ranged from 20.5 °C to 30.8 °C (Fig. 2e), reflecting the tropical climate conditions of the study area (Ligate et al., 2022; WHO, 2022). Most of the surface water samples had pH values that exceeded the WHO guideline of 8.5, suggesting alkaline conditions likely influenced by carbonate-rich rocks, sediment resuspension, or localised runoff and catchment disturbance (WHO, 2022).

Table 1
Dose conversion factor with estimated annual water consumption rate for different age groups.

Age group	Annual water consumption (L year^{-1})	Dose convention factor (Sv Bq^{-1}) per age group (ICRP, 2013)					
		^{238}U	^{234}U	^{235}U	^{226}Ra	^{210}Po	^{210}Pb
Infant <1 y	109.5	3.4×10^{-7}	3.7×10^{-7}	3.5×10^{-7}	4.7×10^{-6}	2.6×10^{-5}	8.4×10^{-6}
Child 1 year	273.75	1.2×10^{-7}	1.3×10^{-7}	1.3×10^{-7}	9.6×10^{-7}	8.8×10^{-6}	3.6×10^{-6}
Child 5 year	365	8.0×10^{-8}	8.8×10^{-8}	8.5×10^{-8}	6.2×10^{-7}	4.4×10^{-6}	2.2×10^{-6}
Child 10 year	365	6.8×10^{-8}	7.4×10^{-8}	7.1×10^{-8}	8.0×10^{-7}	2.6×10^{-6}	1.9×10^{-6}
Teen 12–17 years	547.5	6.7×10^{-8}	7.4×10^{-8}	7.0×10^{-8}	1.5×10^{-6}	1.6×10^{-6}	1.9×10^{-6}
Adult >17 y	730	4.5×10^{-8}	4.9×10^{-8}	4.7×10^{-8}	2.8×10^{-7}	1.2×10^{-6}	6.9×10^{-7}

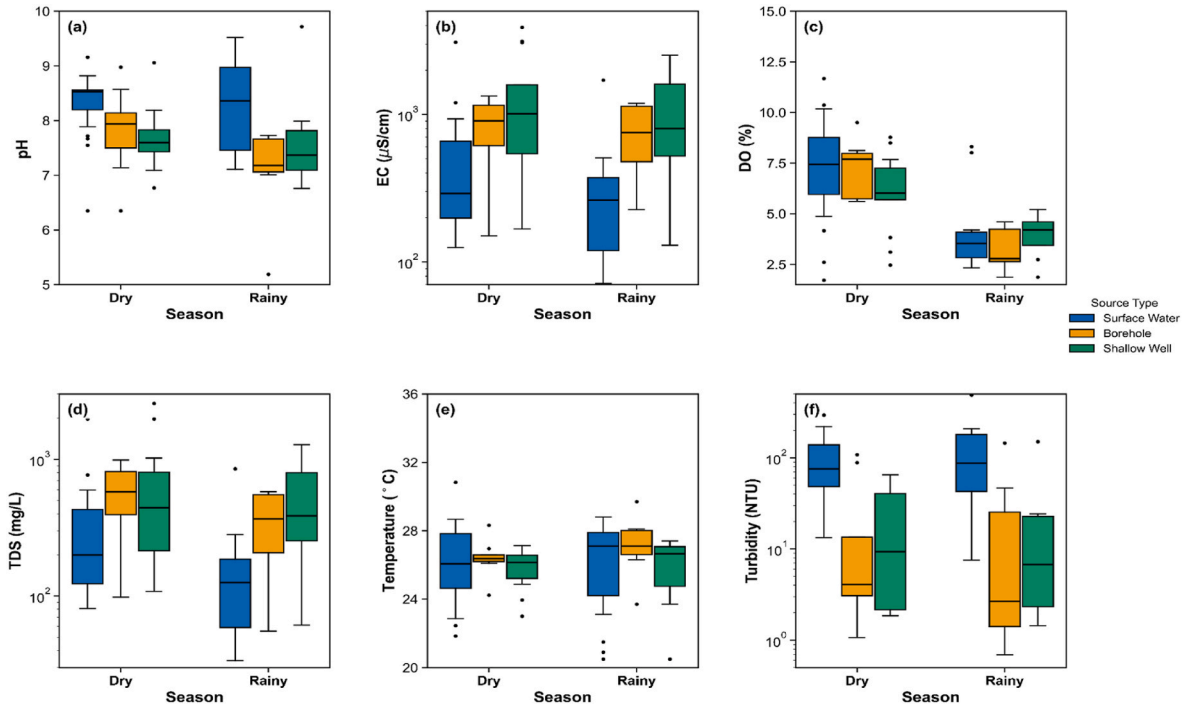

Fig. 2. Boxplots showing seasonal and spatial variations of in-situ water quality parameters in surface water, boreholes, and shallow wells during dry and rainy seasons: (a) pH, (b) electrical conductivity (EC), (c) dissolved oxygen (DO), (d) total dissolved solids (TDS), (e) temperature, and (f) turbidity. Boxes represent the interquartile range (IQR) with the median; whiskers indicate the 10th and 90th percentiles, and filled circles denote outliers. Electrical conductivity, total dissolved solids, and turbidity are presented on logarithmic scales.

However, elevated pH in the shallow well (MR_18) may reflect prolonged water-rock interaction, infiltration of alkaline materials from soil and anthropogenic inputs from surface land where dilution is limited (Kihampa and Wenaty, 2013; Lapworth et al., 2017; Nkinda et al., 2021).

Electrical conductivity (EC) and total dissolved solids (TDS) were generally high, especially in shallow-well and borehole, indicating higher concentrations of dissolved ions (Fig. 2b and d). The higher EC (~3890 µS/cm) and TDS (~2560 mg/l) during dry season were significantly above WHO guideline values for drinking water, suggesting contributions from dissolution of natural minerals, land-use activities, household septic tanks or pit latrines, which intensify solute loading in wells (Al Hatmi et al., 2025; Lapworth et al., 2017). Surface water, at MR_43, also showed elevated EC (~3080 µS/cm) and TDS (~1970 mg/L likely linked to agricultural inputs. Compared to earlier studies in the Mara Basin, the present values indicate increase solute loading, possibly due to intensified land use (Martin et al., 2018; Nkinda et al., 2021),

Dissolved oxygen (DO) levels were notably lower (<4) in most surface water samples during the rainy season (Fig. 2c) consistence with organic enrichment and reduce flow conditions, consistence with previous report from the Mara River basin, where domestic deeds and livestock waste have been identified as contributors to oxygen depletion in surface water (VPO, 2022). Low DO in shallow wells and boreholes likely reflect limited atmospheric oxygen exchange and subsurface oxygen consumption within groundwater systems, with deeper groundwater also indicating longer residence times and more reducing conditions (Becher et al., 2022). Turbidity levels were exceptionally high in all surface water (~622 NTU), and remained elevated in groundwater (Fig. 2f), particularly during rainy season, suggesting poor well construction, unconsolidated aquifer materials, and disturbance of sediments during water abstraction (Lapworth et al., 2017; World Health Organization (WHO), 2022).

3.2. Activity concentration of ^{226}Ra, ^{238}U, ^{235}U, and ^{234}U in water

The measured activity concentrations of ^{238}U, ^{235}U, ^{234}U, and ^{226}Ra in water samples collected from different water sources (surface water, shallow wells, and boreholes) during the rainy and dry seasons are visually illustrated in Fig. 3(a–d) and presented in Tables S 3 and S 4. The seasonal distributions of radionuclides activity concentration (^{226}Ra, ^{238}U, ^{235}U, and ^{234}U) in water sources (surface water, boreholes, and shallow wells) show a clear disparity among the investigated water sources (Fig. 3).

Among other radionuclides, ^{226}Ra (Fig. 3a) depicted the lowest activity concentrations across all water sources in both seasons, due to its relatively low solubility, inability to form soluble complexes in water, and preferential association with particulate and mineral phases (Nuccetelli et al., 2012a). Among all water sources, boreholes depicted the highest activity concentration of ^{226}Ra and ranged from 0.59 mBq/L to 169.7 mBq/L with the median value of 4.19 mBq/L during the rainy season and from 0.4 mBq/L to 107.6 mBq/L with the median value of 5.93 mBq/L during dry season, with peak values at site MR_8 (Table S 4). Moreover, the measured activity concentrations in all water samples were below the WHO drinking water threshold, indicating less radiological concern (World Health Organization (WHO), 2022).

Across all uranium isotopes, activity concentration of ^{234}U, when compared with ^{238}U, portrayed higher concentrations in several sites of investigated water sources, with the highest activity concentrations in groundwater (shallow wells), which in some cases exceeded the WHO threshold limit for drinking water in both seasons (Fig. 3 b and d), indicating radiological concern to the communities relying on shallow wells for drinking. The higher ^{234}U activity concentration when compared with ^{238}U reflects the isotopic disequilibrium between ^{234}U and ^{238}U resulting from the alpha decay-induced recoil process, which reduces its stability by expelling ^{234}U from the mineral lattice (rocks), enhances ^{234}U mobility, and explains its elevated activity concentrations in shallow wells where water-rock interaction and exchange processes are dominant (Kumar et al., 2014, 2016; Tonev et al., 2023). ^{235}U

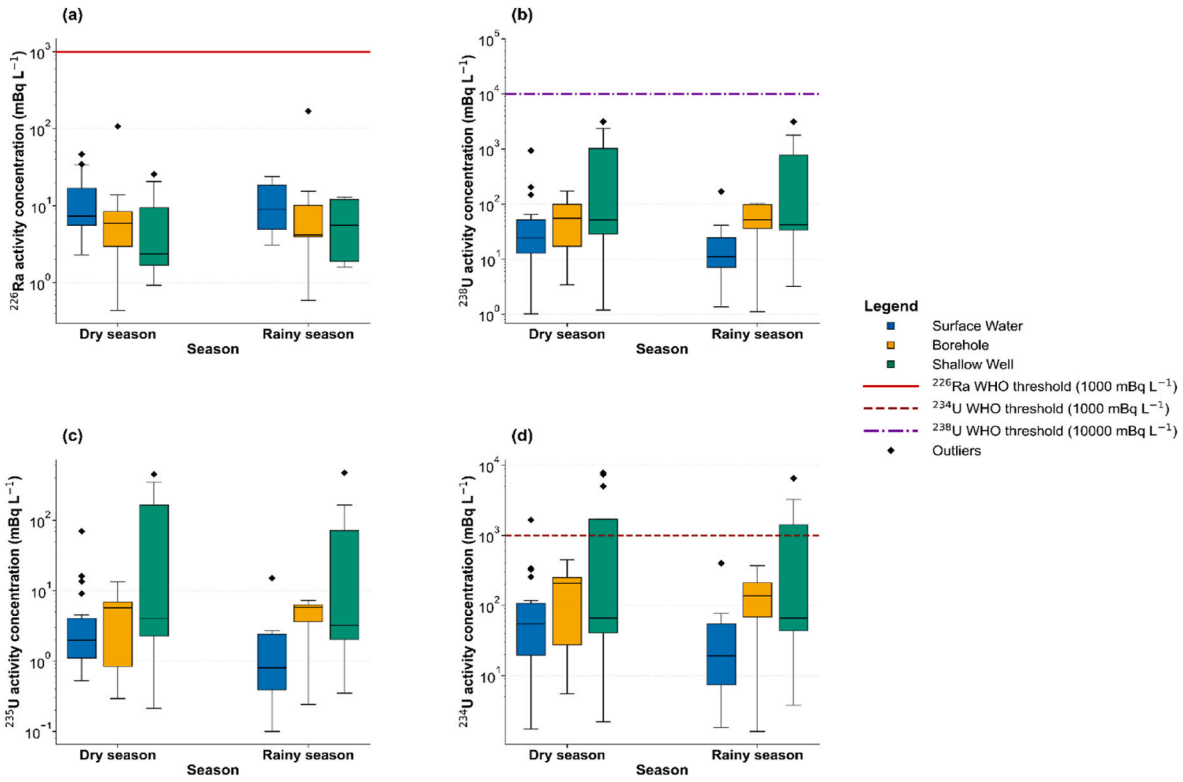

Fig. 3. Activity concentration of (a) ^{226}Ra, (b) ^{238}U, (c) ^{235}U, and (d) ^{234}U in surface water, borehole, and shallow wells during dry and rainy seasons.

activity concentrations remain lower than those of other uranium isotopes (Fig. 3c), yet are higher in shallow wells than in boreholes and surface water during both seasons (Tables S3 and S4).

The activity concentration of ^{235}U in shallow wells ranged from 0.21 to 450 mBq/L during the dry season and from 0.35 to 473 mBq/L during the rainy season with the median of 4.06 mBq/L and 3.22 mBq/L respectively, with the peak at MR_3. ^{238}U and ^{234}U on the other hand, ranged from 1.19 mBq/L to 3150 mBq/L with the median value of 51.8 mBq/L and from 2.19 mBq/L to 7820 mBq/L with the median of 66.4 mBq/L, respectively, during dry season, with extreme concentrations at MR_3, MR_18, MR_20 and MR_21. During rainy season, the activity concentrations of ^{238}U and ^{234}U ranged from 3.2 mBq/L to 3130 mBq/L (median: 41.9 mBq/L) and from 3.8 mBq/L to 6530 mBq/L (median: 66 mBq/L), respectively, with extreme concentrations at the same sites as in dry season.

The higher maximum uranium activity concentration in the identified shallow wells (Table S 4) is likely due to geological characteristics of sampling sites, where the aquifer overlaps granitic lithology, which is naturally uranium-enriched from zircon and monazite uranium-bearing minerals, which ease uranium release into groundwater (Kazimoto and Ikingura, 2014; Mshiu et al., 2008). Moreover, interference from anthropogenic inputs, likely agricultural activities on the surface water, specifically the Mara River, has elevated the activity concentrations of ^{234}U and ^{238}U when compared to other surface water (Mara River tributaries and Mori River) sampling sites (Table S 3). The activity concentration of ^{238}U and ^{234}U ranged from 4.9 to 900 mBq/L with the median value of 53 mBq/L and from 11.3 mBq/L to 1700 mBq/L with the median of 90 mBq/L during dry season, with the extreme peak at MR_43. The measured activity concentrations of ^{234}U exceeding the WHO drinking water screening level indicate potential annual ingestion doses above the reference value of 0.1 mSv/y solely from that radionuclide, thereby necessitating further risk assessments and monitoring to determine whether they pose unacceptable adverse radiological effects to the population relying on them for drinking water. In oxidizing conditions, uranium can form soluble stable complexes (eg. with carbonates) and can move for a long distance, while in reducing conditions (absence of air), it precipitates, forming concentrated secondary deposits (Nuccetelli et al., 2012a; Rovan et al., 2021).

A correlation analysis (Table 2) revealed a seasonal shift between uranium isotopes, ^{226}Ra, and water parameters, suggesting that shallow wells are particularly vulnerable to hydrogeochemical variations and surface-derived influence. During the rainy season, significant positive correlations were observed between ^{234}U and ^{238}U ($\rho = 0.93$; $p = 0.05$) and between uranium isotopes, TDS, and EC ($\rho = 0.81$; $p = 0.015$). This relationship indicates that uranium isotopes transported to shallow wells through fractures, faults, and weathered rock zones are largely controlled by ionic strength and salinity-driven complexation. The strong association between U, EC and TDS agrees with recent work reporting high U-TDS and U-EC correlations in contaminated groundwater (Cho and Choo, 2019; Kaur Guron et al., 2025).

Elevated dissolved solids may also reflect anthropogenic inputs from nearby household septic systems and pit latrines, which intensify solute loading in wells and enhance uranium mobility in groundwater (Al Hatmi et al., 2025; Lapworth et al., 2017; Rovan et al., 2021; Tonev et al., 2023). In contrast, ^{226}Ra exhibited only weak correlations with EC and TDS ($\rho = 0.48$; $p < 0.05$), suggesting that radium mobilisation is governed by different geochemical mechanisms, including adsorption-desorption processes, co-precipitation, and mineral surface interactions, rather than simple (Zhang et al., 2025).

During dry season, uranium isotopes (^{238}U, ^{235}U, and ^{234}U) showed a strong positive correlation with temperature (ρ = 0.66-0.68), pH ($\rho = 0.63$-0.64), and EC ($\rho = 0.75$-0.81), indicating enhanced uranium mobility under warmer, more alkaline conditions. These relationships likely reflect the combined effect of prolonged water-rock interaction, high evaporation, and reduced dilution (Al Hatmi et al., 2025; Lapworth et al., 2017). A significant positive correlation between turbidity and dissolved oxygen ($\rho = 0.55$) and a weak negative correlation with uranium isotopes ($\rho = -0.17$ to - 0.26), suggest that particulate interactions may partially remove uranium from solution through adsorption or co-precipitation processes. The consistently strong positive correlation

Table 2
Spearman correlation matrix between ^{226}Ra, uranium isotopes and physico chemical parameters of water (pH, EC, DO, TDS and Turbidity) during Rainy and dry season.

Season	Parameters	Temperature	pH	EC	DO	TDS	Turbidity	^{226}Ra	^{238}U	^{235}U	^{234}U
Rain season	Temperature	1									
	pH	0.69	1								
	EC	**0.77**	0.29	1							
	DO	0.13	−0.07	0.07	1						
	TDS	**0.77**	0.29	**1.00**	0.07	1					
	Turbidity	0.27	**0.79**	−0.3	−0.06	−0.3	1				
	^{226}Ra	0.29	0.1	0.48	−0.29	0.48	0.24	1			
	^{238}U	0.62	0.36	**0.88**	−0.17	**0.88**	−0.07	0.48	1		
	^{235}U	0.62	0.36	**0.88**	−0.17	**0.88**	−0.07	0.48	**1.00**	1	
	^{234}U	0.62	0.33	**0.81**	−0.05	**0.81**	−0.1	0.4	**0.93**	**0.93**	1
		Temperature	pH	EC	DO	TDS	Turbidity	^{226}Ra	^{238}U	^{235}U	^{234}U
	Temperature	1									
Dry season	pH	**0.58**	1								
	EC	**0.59**	**0.71**	1							
	DO	−0.3	0.09	0	1						
	TDS	**0.55**	0.22	0.36	0.05	1					
	Turbidity	−0.51	−0.05	−0.42	**0.55**	−0.32	1				
	^{226}Ra	0.34	0.51	0.26	−0.32	0.34	0.14	1			
	^{238}U	**0.66**	**0.63**	**0.75**	−0.05	0.32	−0.17	0.38	1		
	^{235}U	**0.68**	**0.64**	**0.81**	−0.09	0.38	−0.26	0.42	**0.98**	1	
	^{234}U	**0.66**	**0.63**	**0.75**	−0.05	0.32	−0.17	0.38	**1.00**	**0.98**	1

** = statistically significant at $p < 0.01$.

among uranium isotopes in both seasons further indicates a common lithogenic origin and coupled mobilization behaviour, as reported in other groundwater systems affected by natural weathering processes (He et al., 2022a; Kumar et al., 2016).

To further evaluate the relationship between radionuclides and physico-chemical parameters identified by the correlation analysis, and to identify the dominant hydrogeochemical processes controlling radionuclide distributions, principal component analysis (PCA) was performed (Fig. 4). The first two principal components explained 57.01% of the total variance, with PC1 and PC2 accounting for 40.36% and 16.65%, respectively (Fig. 3a). The PCA biplot showed a clear separation between dry- and rainy-season samples, confirming that seasonal hydrological conditions strongly influence groundwater chemistry and radionuclide mobility. Shallow-well samples were more widely dispersed across the ordination space than borehole samples, indicating greater hydrochemical variability and a stronger

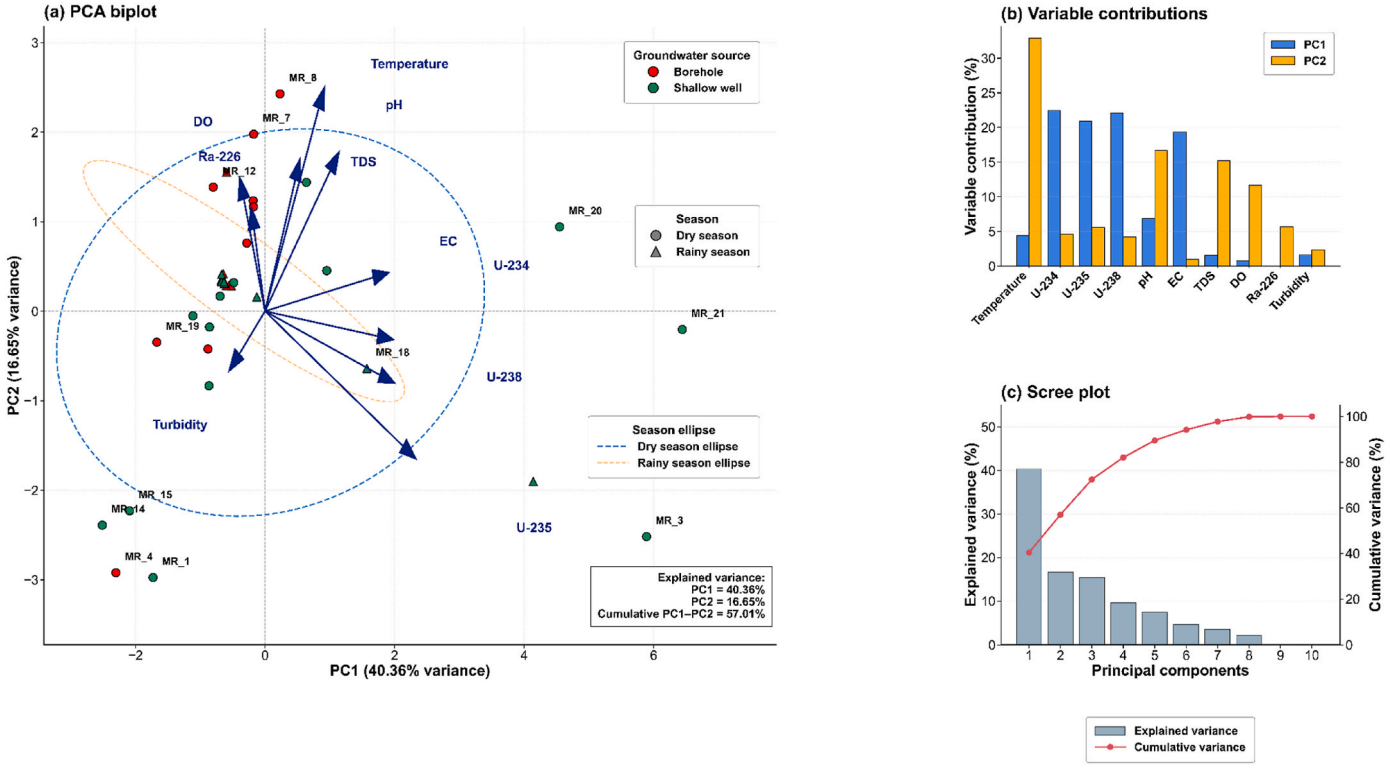

Fig. 4. Principal component analysis (PCA) of radionuclides and physicochemical parameters in groundwater from mining-impacted areas of northern Tanzania during the dry and rainy seasons: (a) PCA biplot showing sample distribution, variable loadings, and seasonal ellipses; (b) variable contributions to PC1 and PC2; and (c) scree plot showing explained and cumulative variance.

susceptibility to surface-derived inputs.

The clustering of uranium isotopes (^{234}U, ^{235}U, and ^{238}U) showed positive loadings with EC and TDS on PC1, indicating that uranium occurrence is mainly governed by groundwater mineralisation and water-rock interaction, in line with previous multivariate studies of natural radioactivity in groundwater (Abou Zakhem et al., 2017; Matiatos et al., 2014; Tanasković et al., 2012). This is consistent with the strong positive correlations between uranium and dissolved constituents in shallow wells (Table 2), suggesting that prolonged contact with U-bearing lithologies enhances uranium mobilization (Baják et al., 2022; Cho and Choo, 2019; Kaur Guron et al., 2025). Several shallow-well samples, particularly MR_20 and MR_21, plot towards the positive side of PC1, reflecting elevated uranium activities and higher dissolved ion concentrations. This pattern implies localized uranium enrichment and emphasizes the role of lithology and residence time, similar to observations in other fractured and granitic aquifers (Baják et al., 2022; Cho and Choo, 2019; Kaur Guron et al., 2025).

The second principal component (PC2) was dominated by temperature, pH, and dissolved oxygen, indicating an additional control by physicochemical conditions. The association of uranium isotopes with temperature and pH further supports the dry-season correlations and suggests enhanced uranium mobility under alkaline conditions through stable aqueous complexes, as documented in carbonate-rich and oxidizing aquifers (Baják et al., 2022; Choi et al., 2022; Vengosh et al., 2022). In contrast, ^{226}Ra exhibited a distinct loading pattern and showed a closer association with turbidity and dissolved oxygen, indicating that radium was strongly influenced by adsorption-desorption and barite/Fe-oxide-related processes, rather than the same mineralisation trends that govern uranium (Tanasković et al., 2012; Vengosh et al., 2022). The resulting disequilibrium between U isotopes and Ra-226 is widely reported, reflecting their different responses to redox conditions, mineralogy and groundwater flow systems (Baják et al., 2022; Vengosh et al., 2022).

Although groundwater from shallow wells and boreholes partly overlapped in conferment space, shallow wells displayed greater variability in radionuclide activities and hydrochemical composition, indicating higher sensitivity to surface influences, recharge, and short flow paths, as also observed in other multivariate groundwater assessments (Abou Zakhem et al., 2017; Baják et al., 2022; Matiatos et al., 2014). Borehole samples clustered closer to the centre of the PCA, suggesting more stable hydrochemical conditions and lower variability. The substantial overlap between dry and rainy season samples indicates that radionuclide distributions are controlled predominantly by subsurface geochemical processes rather than short-term seasonal changes, in agreement with studies where mineralisation and redox evolution outweigh immediate recharge effects (Abou Zakhem et al., 2017; Baják et al., 2022; Matiatos et al., 2014).

These findings underscore the key role of aquifer geochemistry in regulating radionuclide mobility and show that shallow groundwater systems are more responsive to hydrogeochemical variations than deeper borehole waters (Abou Zakhem et al., 2017; Matiatos et al., 2014; Tanasković et al., 2012). While proximity to mining activities was not explicitly evaluated, future studies incorporating distance-to-mine analyses could help further distinguish mining-related influences from natural geogenic controls.

3.3. Seasonal variability of $^{234}U/^{238}U$ activity ratios in water

The natural uranium consists predominantly of ^{238}U (~99.275% by mass), with minor contributions from ^{235}U (~ 0.72%), and trace amounts of ^{234}U (~ 0.005%) (Kumar et al., 2014; UNSCEAR, 2000). Literature reports that $^{234}U/^{238}U$ activity ratios in natural water are often close to unity, although they can also exceed unity under certain conditions (Boryło and Skwarzec, 2014; Kumar et al., 2014, 2016). The activity ratio of $^{234}U/^{238}U$ in the examined water samples shows distinct variations across water sources (surface water, borehole, and shallow wells) during the dry and rainy season (Fig. 5 and Tables S3–5).

The results show that the activity ratios of $^{234}U/^{238}U$ in most sites were greater than 1, surpassing secular equilibrium, confirming preferential mobilisation of ^{234}U relative to ^{238}U due to alpha recoil processes and radiation-induced crystal lattice damage, which promote the preferential release and leaching of ^{234}U from the mineral matrices into the aqueous phase (He et al., 2022b; Mourad et al., 2021; Nuccetelli et al., 2012b; Rovan et al., 2021; Tonev et al., 2023). During dry and rainy season, the highest $^{234}U/^{238}U$ activity ratios depicted on boreholes ranged from 1.31 to 4.39 and from 1.31 to 3.71, with median values of 2.52 and 2.31 respectively, followed by surface water (range: 0.92-3.93 and 0.9-2.72 with median of 1.73 and 1.79) while shallow wells show lower ratios, though still above the 1 in most sites (range: 0.9 - 2.48 and 0.6 - 2.09 with the median of 1.66 and 1.59). These activity ratio values lie within the reported ranges of 0.51 - 9.02 (Boryło and Skwarzec, 2014).

The elevated ratios in boreholes (MR_5, MR_7, MR_10, MR_16 and MR_17), reflect the accumulation of dissolved ^{234}U or direct alpha recoil from the soils or carbonated rocks into the aqueous phase, prolonged groundwater times and water-rocks interaction, while moderate ratios from surface water especially from Mara river tributaries (MR_25 and MR_39) reflect shorter interaction times and rapid hydrological flushing, whereas relative lower ratios in shallow wells indicate mixing between newly recharged water and pre-existing groundwater. Generally, high and low $^{234}U/^{238}U$ activity ratios are due to enrichment and depletion of ^{234}U in groundwater (boreholes and shallow wells), which depends on the uranium abundance under several geochemical settings during the alpha recoil process (He et al., 2022a; Kumar et al., 2014; Rovan et al., 2021).

3.4. Activity concentration of ^{226}Ra, ^{238}U, ^{234}U, ^{210}Po and ^{210}Pb in fish tissues

Activity concentration of analysed radionuclides (^{226}Ra, ^{238}U, ^{235}U, ^{234}U, ^{210}Po, and ^{210}Pb) of sampled fish tissues (flesh, bones and gills) is presented in Table 3. Due to differences in feeding habits among fish species (Tilapia, Catfish, and African Lungfish), variations in activity concentration among fish tissues were observed. Among all analysed tissues, ^{238}U and ^{234}U showed the lowest activity concentrations in flesh (muscles), with mean activities ranged from 0.06 to 0.71 Bq/kg and from 0.12 to 0.43 Bq/kg, respectively, while higher values were detected in Tilapia bones and gills (Table 3). Despite having less information regarding uranium isotope levels in fish tissues specifically from Africa, the measured activity concentration of ^{238}U in fish from Mara River, Tanzania, was lower than that reported by Fasae and Isinkaye (2018). The activity ratios of $^{234}U/^{238}U$ from freshwater fish tissues (Table 3) are

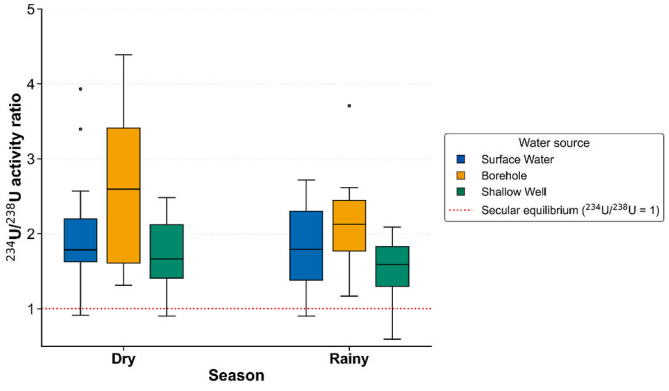

Fig. 5. Seasonal variation of $^{234}U/^{238}U$ activity ratio across surface water, boreholes, and shallow wells during dry and rainy seasons. The threshold 1 shown by the dotted line indicates ^{234}U in secular radioactive equilibrium with ^{238}U. Values below or above the line indicate that this equilibrium is disrupted.

Table 3
Activity concentration of radionuclides (Bq/kg) in fish tissues (flesh, bones and gills) samples collected from Mara River with combined standard uncertainties (k = 1).

Sample ID	Sample name	Tissue	Activity concentrations of fish tissues (Bq/kg dry weight) ± standard deviation (SD)					Activity ratios	
			^{238}U	^{234}U	^{226}Ra	^{210}Po	^{210}Pb	^{210}Po/^{210}Pb	^{234}U/^{238}U
16/25	Tilapia	Flesh	0.21 ± 0.04	0.39 ± 0.05	0.11 ± 0.02	0.64 ± 0.16	28 ± 5.1	0.03	2.48
17/25			0.14 ± 0.03	0.46 ± 0.06	0.6 ± 0.059	0.73 ± 0.18	16.1 ± 2.7		
Mean ± SD			**0.17 ± 0.04**	**0.43 ± 0.06**	**0.36 ± 0.042**	**0.68 ± 0.17**	**22 ± 3.9**		
16/25B		Bones	1.81 ± 0.12	2.72 ± 0.16	2.22 ± 0.17	0.53 ± 0.47	15.7 ± 9.9	0.03	1.6
17/25B			1.39 ± 0.11	2.4 ± 0.16	3.0 ± 0.21	0.86 ± 0.35	31 ± 9.0		
Mean ± SD			**1.6 ± 0.12**	**2.56 ± 0.16**	**2.61 ± 0.19**	**0.69 ± 0.41**	**23.4 ± 9.5**		
16/25G		Gills	1.71 ± 0.12	3.56 ± 0.19	0.85 ± 0.10	2.26 ± 0.56	48.8 ± 8.5	0.06	2.11
17/25G			2.38 ± 0.15	5.1 ± 0.25	1.4 ± 0.13	3.4 ± 0.97	40.4 ± 8.1		
Mean ± SD			**2.05 ± 0.13**	**4.33 ± 0.22**	**1.13 ± 0.12**	**2.85 ± 0.77**	**44.6 ± 8.3**		
18/25	Catfish	Flesh	0.14 ± 0.04	0.15 ± 0.04	0.12 ± 0.03	1.52 ± 0.36	20.2 ± 3.4	0.11	1.47
19/25			0.05 ± 0.03	0.14 ± 0.05	0.15 ± 0.03	2.23 ± 0.55	15.2 ± 2.7		
Mean ± SD			**0.10 ± 0.03**	**0.14 ± 0.05**	**0.14 ± 0.029**	**1.88 ± 0.46**	**17.7 ± 3.0**		
18/25B		Bones	0.58 ± 0.06	0.96 ± 0.08	0.98 ± 0.13	0.87 ± 0.43	41.2 ± 14.4	0.04	1.69
19/25B			0.39 ± 0.05	0.68 ± 0.07	0.65 ± 0.10	2.82 ± 0.61	62.9 ± 9.6		
Mean ± SD			**0.49 ± 0.057**	**0.82 ± 0.07**	**0.82 ± 0.11**	**1.84 ± 0.52**	**52.1 ± 12**		
20/25	African Lungfish	Flesh	0.11 ± 0.02	0.08 ± 0.03	**0.092** ± 0.02	2.43 ± 0.39	26.6 ± 3.0	0.09	1.80
21/25			0.02 ± 0.02	0.16 ± 0.04	**0.07** ± 0.02	1.87 ± 0.43	22.9 ± 3.8		
Mean ± SD			**0.06 ± 0.02**	**0.12 ± 0.03**	**0.081 ± 0.02**	**2.15 ± 0.44**	**24.7 ± 3.4**		

above 1, mirroring the pattern observed in water samples (Table S3) as a result of preferential mobilisation of ^{234}U relative to ^{238}U due to alpha recoil effect, which cause equilibrium disruption in soil and water as a result of preferential release and leaching of ^{234}U from the mineral matrices to the environment (Nuccetelli et al., 2012b; Štrok and Smodiš, 2011c).

The highest mean activity concentration of ^{226}Ra was recorded in Tilapia bones (2.61 ± 0.20 Bq/kg) and gills (1.13 ± 0.12 Bq/kg), consistent with preferential accumulation in mineralized skeletal tissues and water-contact organs. Similar bone-dominant patterns of ^{226}Ra have been reported in freshwater and marine fish species, in which skeletal tissues exhibit substantially higher levels than muscle tissues (Donaher et al., 2023; Lacroix-Durand et al., 2025). This behaviour reflects the chemical similarity of ^{226}Ra to Ca^{2+}, enabling its incorporation into the mineral phase of bone during skeletal mineralisation (Donaher et al., 2023; Jeffree and Simpson, 1986; Jeffree and Simpsonf, 1984).

In contrast, lower activity concentration measured on African Lungfish flesh (0.081 ± 0.020) indicated minimal incorporation into flesh (muscle) tissue. Overall, the measured activity concentration of ^{226}Ra in fish from Mara River were lower than those reported for fish from Lake Manyara (7.61 ± 0.21Bq/kg), Tanzania, Lake Edward (12.76 to 18.73 Bq/kg) from Uganda and from Eleyele Reservoir (21.65 ± 1.83 Bq/kg) from Nigeria (Kazoka et al., 2023; Sunday et al., 2025; Uzorka et al., 2025), highlighting spatial variability linked to geochemical conditions and environmental settings. The moderate activity concentrations in edible fish tissues have been observed for ^{210}Po, ranging from 0.68 ± 0.17 for Tilapia flesh to 2.15 ± 0.44 Bq/kg for African Lungfish flesh. Across all fish species and tissues, ^{210}Pb depicted the highest activity concentrations and ranged from 17.7 ± 3.0 Bq/kg (Catfish flesh) to 24.7 ± 3.4 Bq/kg (African Lungfish flesh), and from 23.4 ± 9.5 Bq/kg (Tilapia bones) to 52 ± 12 Bq/kg (Catfish bones).

The prevalence of ^{210}Pb relative to ^{210}Po in fish tissues reveals the characteristic behaviour of natural radionuclides in freshwater systems, where exposure pathways are controlled by sediment-water interactions and dietary uptake (IAEA, 2010; UNSCEAR, 2016). The findings of this study are in agreement with the reported literature values for freshwater fish for ^{210}Po, which ranged from 0.079 to 3.08 Bq/kg, and from 0.014 to 3 Bq/kg fresh weight for ^{210}Pb (Al-Masri et al., 2000; Štrok and Smodiš, 2011b), though the activity concentration of ^{210}Pb in this study is generally higher than those from the reported literature. The ^{210}Po/^{210}Pb activity ratios measured in fish tissues were consistently less than a unit (ranging from 0.03 to 0.11), confirming the predominance of ^{210}Pb accumulation in fish over ^{210}Po in the Mara River aquatic environment. The low ratios can be attributed to lower ^{210}Po activity concentrations in water compared to ^{210}Pb (Štrok and Smodiš, 2011a), reflecting the strong particle-reactive behaviour of ^{210}Pb, thereby enhancing its transfer to aquatic organisms through gill contact and sediment-related feeding pathways (IAEA, 2010; UNSCEAR, 2016). The findings of this study are consistent with those of Štrok and Smodiš (2011a). In general, due to insufficient radioecological data for African fish species, particularly for fish tissue in aquatic environments, direct comparisons are not possible.

3.5. *Total annual effective dose (AED) and excess life cancer risk (ELCR) due to ingestion of ^{226}Ra, ^{238}U, ^{235}U, and ^{234}U in water*

The total annual effective ingestion doses (in mSv/year) estimated for the selected critical groups of the population; infants (<1 year), children (1, 5, 10 and 12-17 years), and adults (>17 years) based on the obtained activity concentration of analysed radionuclides in water are presented in Figs. 6 and 7 and Tables S5 and S6. Based on the given results, the consumption of water from shallow wells exhibited the largest total annual effective dose with large variability, particularly among children, as shown in Fig. 6b and Table S5.

The AEDs for consumption of water from shallow wells ranged from $\sim 10^{-4}$ mSv/year to values that surpassed the ICRP-recommended public dose of 1 mSv/y (at MR_3) and WHO drinking water screening dose of 0.1 mSv/y at some locations, with a maximum dose of 1.17 mSv/year observed for a 5-year-old child (ICRP, 2013; World Health Organization, 2011, 2022). Consumption of water from boreholes results in AEDs with a typical range of ~10-3 mSv/y to $\sim 10^{-1}$ mSv/y with maximum total AEDs of 0.127 mSv/y observed for teens (12-17 years) (Fig. 7d) at MR_8 (Table S 5).

Moderate total AED values were observed in adults (Fig. 6c), with shallow wells exceeding the WHO screening level of 0.1 mSv/y at several sites. The observed total AEDs exceeding 1 mSv/y at several locations is likely due to elevated activity concentrations of radionuclides in water and higher water ingestion rates in adults, which can offset their lower dose conversion factors compared with children.

Consumption of water from surface water, on the other hand, would result in intermediate AEDs with elevated values of 0.165 mSv/y over a 5-year period (Fig. 7b) at MR_43 on the Mara River (Table S6), indicating localised radiological hotspots. The higher dose in children clearly indicate that children are the most vulnerable group to radiation hazard due to their intensive growth and development of different body organs and bones.

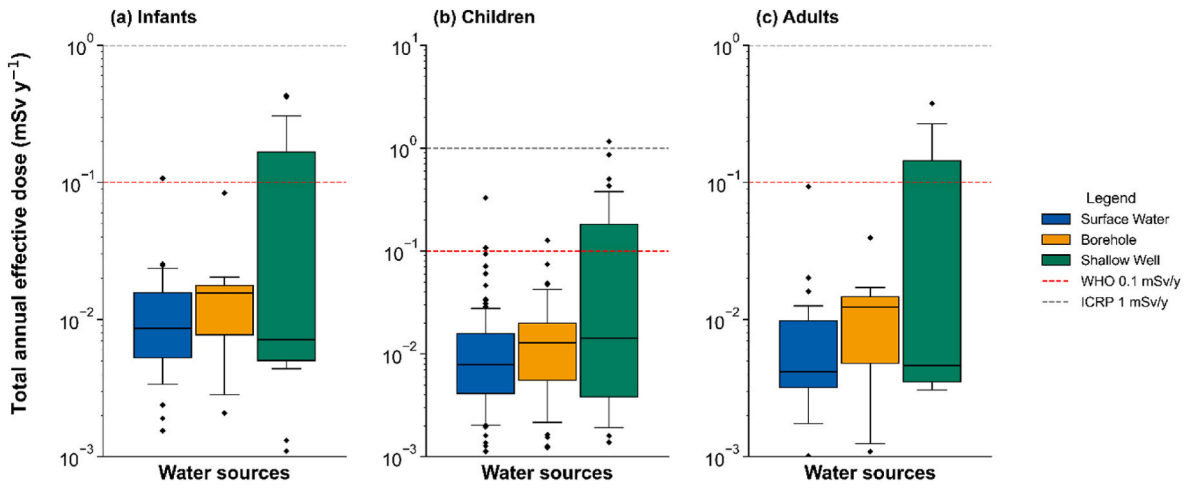

Fig. 6. Total annual effective dose for (a) infants, (b) children (1-17 years), and (c) Adults due to ingestion of surface water, and groundwater (borehole and shallow wells).

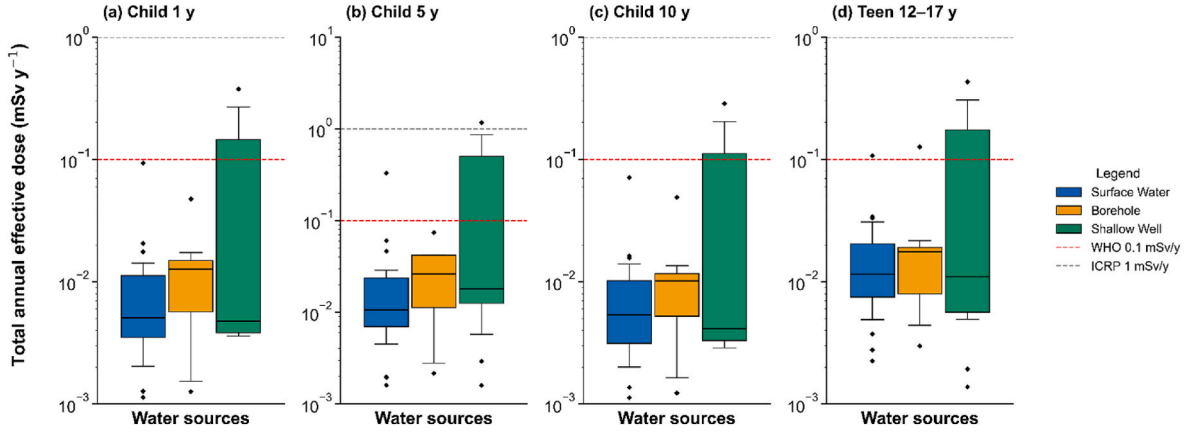

Fig. 7. Total annual effective dose to analysed children age groups due to ingestion of water.

Sampling locations with higher total AEDs for all age groups also indicated higher EC and TDS, confirming prolonged water-rock interaction and solute concentrations driven by evaporation. Generally, specific wells have been identified as having significantly higher radionuclide activity concentrations and could be problematic to use as drinking water sources.

The contribution of each analysed radionuclide to the total annual effective dose for each age group, shown in Fig. 8(a–c), indicates variability of radionuclides (^{226}Ra, ^{238}U, and ^{234}U) activity concentrations in shallow wells, as well as variability in dose conversion factors among them and among different age groups. Across all age groups, uranium isotopes contribute most to the total AEDs at the sampling locations with higher doses (MR_3, MR_18, MR_20, and MR_21), with the largest contributions from ^{234}U followed by ^{238}U, while ^{226}Ra is a secondary but locally important contributor to the wells with lower AEDs. The results show that, for infants and children, ^{234}U contributed more than 70% of contribution to the total dose. Adults, on the other hand, show a similar pattern to children. ^{226}Ra as a secondary contributor in sites with higher AEDs contributed to about 40-98% at sampling sites with lower AEDs, supporting the need for radionuclide-specific and age-dependent risk assessment in gold-mining impacted groundwater systems.

The radionuclides assessed in drinking water samples (^{226}Ra, ^{238}U, and ^{234}U) are predominantly alpha emitters, which have high linear energy transfer (LET), and can deposit large amount of energy over a short distance in biological tissues, and therefore have a greater relative biological effectiveness per unit absorbed dose than beta particles. In contrast, beta particles deposits energy less densely and travel farther through biological tissues, resulting in their lower biological effectiveness per unit absorbed dose than alpha particles. For radiological protection purpose, radiation factor of 20 and 1 are assigned to alpha and beta particles. Nevertheless, the relative contribution of each radionuclide to the total annual effective dose is governed not only by its radiation type but also by its activity concentration in water, its corresponding ingestion dose coefficient, absorption and retention in the body tissues (IAEA, 2014; ICRP, 2013).

The excess lifetime cancer risk (ELCR) associated with ingestion of radionuclides in drinking water was estimated from annual effective doses using age-specific intake rates and dose coefficients. The calculated ELCR values ranged from 3.09×10^{-6} to 1.59×10^{-3}, with a median of 2.35×10^{-5}. The minimum and median ELCR values fall within the range commonly reported for naturally occurring radionuclides in drinking water and are consistent with observations from other regions worldwide, indicating a low radiological cancer risk to consumers (ICRP, 2007a; P. Banzi, 2016b). The maximum ELCR value exceeds the commonly applied radiological risk screening range of 10^{-6} – 10^{-4} used in environmental assessment (ICRP, 2007a). This upper-bound estimate reflects elevated radionuclide concentrations at a limited number of sampling sites rather than typical regional exposure conditions.

When comparing these results with cancer risk associated with cigarette smoking despite different methodology, epidemiological studies and mechanistic models indicate that ELCR for heavy smokers is

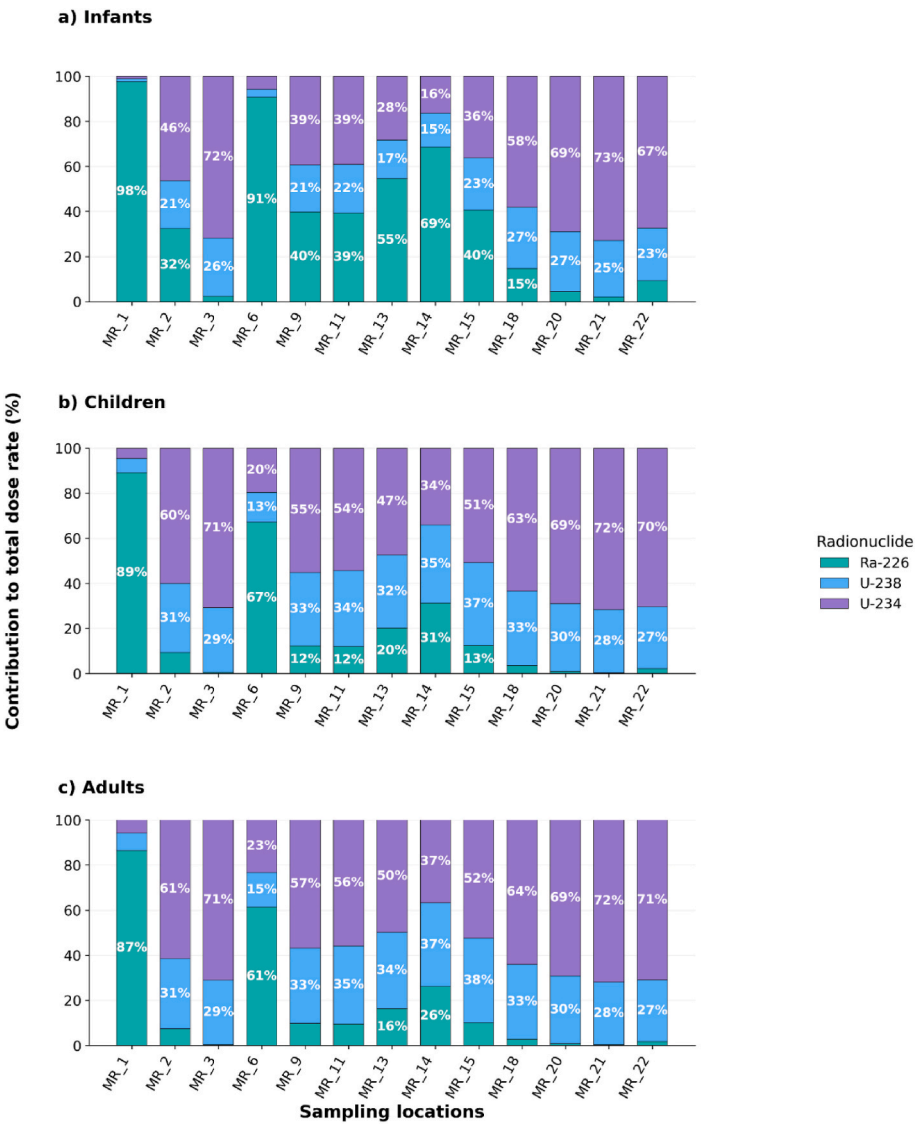

Fig. 8. Percentage contribution of ^{226}Ra, ^{238}U, and ^{234}U in shallow wells for a) Infants, b) Children, and c) Adults during dry season.

typically on the order of 0.2 – 0.6 (Stabile et al., 2017). These values are of several orders of magnitude greater than ELCR estimates for radionuclide ingestion in the assessed drinking water.

(10^{-6} – 10^{-4}). This comparison provides context for the magnitude of radiological risk and demonstrates that the incremental cancer risk from studied radionuclides from drinking-water ingestion in the study area is relatively low, however there is a need for continued monitoring of sites exhibiting higher radionuclides activity concentration level, as well as to include other natural radionuclides, which might be present in drinking water, such as ^{210}Pb, ^{210}Po, ^{230}Th, ^{232}Th and ^{228}Ra, and were out of scope of this study due to logistical limitations.

3.6. Age dependence of total annual effective dose (AED) and excess life cancer risk (ELCR) due to ingestion of ^{226}Ra, ^{238}U, ^{234}U, ^{210}Po, and ^{210}Pb in fish

The total annual effective ingestion dose (AED) resulting from consumption of Tilapia, Catfish, and African lungfish are presented in Table 4 and illustrated in Fig. 9. Across all age groups, African lungfish consistently produced the highest annual effective dose (AED), followed by tilapia, with catfish contributing the lowest. AEDs for lungfish ranged from 1.06 to 3.61 mSv y^{-1}, compared with 0.87-2.80 mSv y^{-1} for Tilapia and 0.78-2.71 mSv y^{-1} for Catfish. The calculated AED exceeded the recommended ICRP public dose reference level of 1 mSv y^{-1} in several age groups, particularly infants, children, and teenagers.

Table 4
Annual effective dose (mSv/y) due to consumption of radionuclides in fish based on age groups.

Age group	Annual effective ingestion dose of fish species (mSv/y)		
	Tilapia	Catfish	African Lungfish
Infant <1 y	2.8	2.71	3.61
Child 1 y.	2.31	2.17	2.91
Child 5 y	1.40	1.28	1.73
Child 10 y	1.19	1.04	1.42
Teen 12–17 y	2.35	1.99	2.73
Adult >17 y	0.87	0.78	1.06

A pronounced age dependence was observed in the estimated ingestion doses. Infants (<1 year) received the highest AEDs, ranging from 2.71 mSv y^{-1} for catfish to 3.61 mSv y^{-1} for African lungfish. One-year-old children exhibited slightly lower AEDs (2.17-2.91 mSv y^{-1}), which declined further in 5-year-old children (1.28-1.73 mSv y^{-1}). The lowest AEDs among paediatric groups were observed in 10-year-old children (1.04-1.42 mSv y^{-1}). AEDs then increased again in teenagers (1.99-2.73 mSv y^{-1}) before decreasing to 0.78-1.06 mSv y^{-1} in adults.

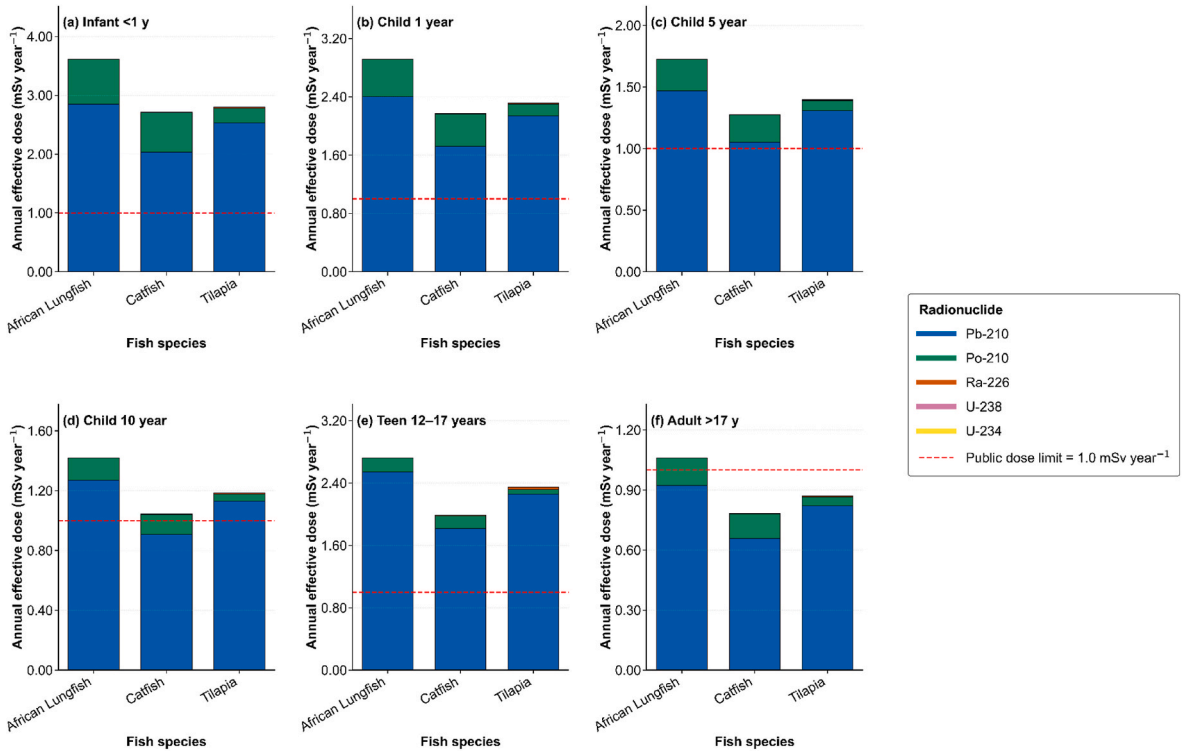

Fig. 9. Age-dependent annual effective dose due to consumption of African Lungfish, Catfish, and Tilapia from the Mara River.

This age-dependent pattern primarily reflects differences in age-specific ingestion dose coefficients and physiological sensitivity, with younger age groups receiving higher doses per unit intake of radionuclide than adults (ICRP, 2013).

The consistent species-dependent pattern (African lungfish > Tilapia > Catfish) reflects differences in feeding ecology and

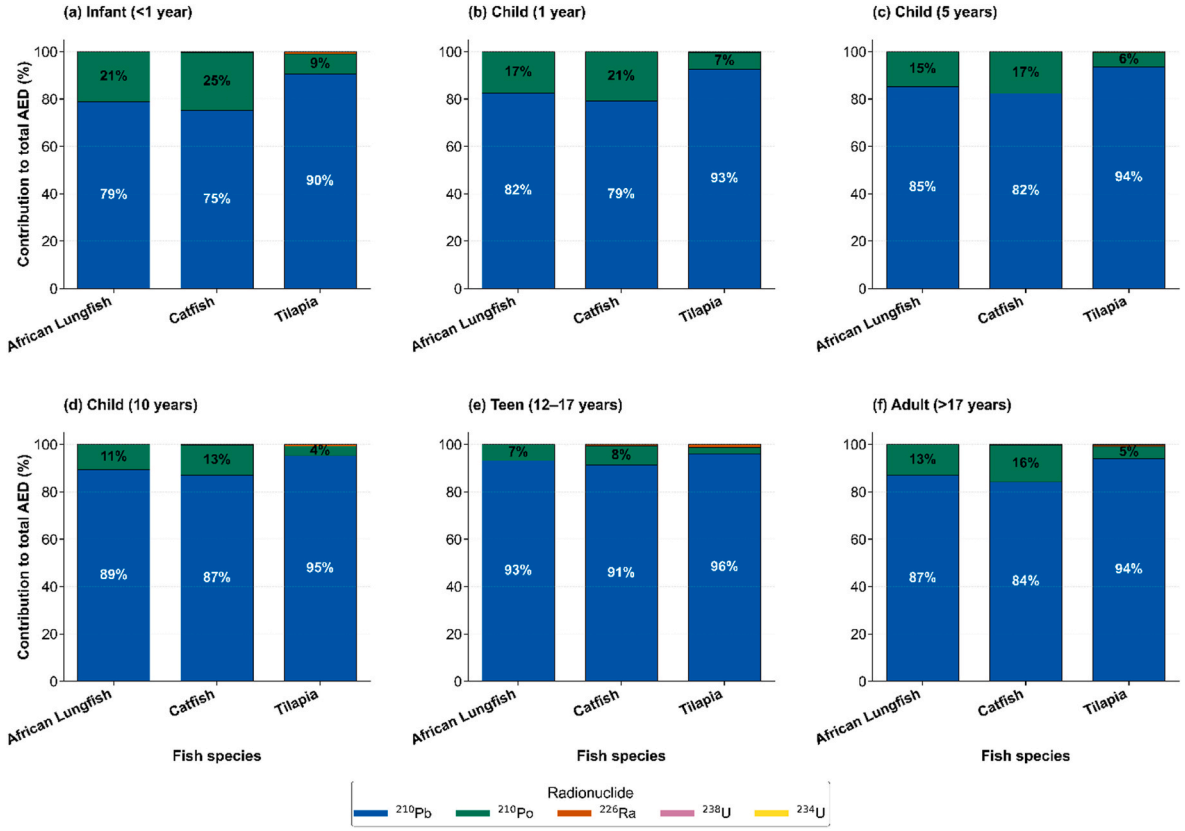

Fig. 10. Percentage contributions of particular radionuclides to the combined effective annual ingestion dose due to fish consumption.

radionuclide bioaccumulation behaviour. African lungfish, as benthic species with frequent contact with bottom sediments, are more likely to accumulate sediment-associated radionuclides, resulting in systematically higher ingestion doses and lifetime cancer risks than the other fish species examined (Nteziyaremye and Omara, 2020). Tilapia exhibited intermediate exposure levels, whereas Catfish showed comparatively lower radionuclide uptake and associated radiological risk, consistent with observations reported by Kazoka et al. (2023) and Temesgen et al. (2022).

The estimated excess lifetime cancer risks (ELCRs) of 3.99×10^{-3}, 3.65×10^{-3}, and 4.99×10^{-3} for Tilapia, Catfish, and African lungfish, respectively, exceeded the USEPA acceptable lifetime cancer risk range of 10^{-6}-10^{-4} (U.S. EPA, 1989). These elevated risks are primarily attributable to the cumulative effects of long-term consumption and the dominant contribution of ^{210}Pb and ^{210}Po to the total ingestion dose. Although the estimated ELCRs remain substantially lower than the lifetime cancer risks associated with heavy smoking, which have been reported to range between 0.2 and 0.6 (Stabile et al., 2017), they indicate a non-negligible radiological risk from chronic fish consumption. Furthermore, the ELCRs associated with fish ingestion were considerably higher than those estimated for drinking water consumption in the same study area, highlighting fish consumption as the more important ingestion pathway for long-term radionuclide exposure. These findings underscore the need for continued radiological monitoring of aquatic food resources in mining-impacted regions.

The contribution of individual radionuclides to total AED varied across fish species but was consistently dominated by ^{210}Pb and ^{210}Po (Fig. 10). ^{210}Pb accounted for approximately 75% - 96% of the total AED, whereas ^{210}Po contributed between 4% and 25%, while the combined contribution of ^{234}U, ^{238}U, and ^{226}Ra was generally less than 1%. The combined contribution of ^{210}Pb and ^{210}Po exceeded 99% of the total AED across all fish species and age groups, demonstrating that these radionuclides are the dominant drivers of radiological exposure associated with fish consumption in the Goldmining region. In contrast, uranium isotopes and ^{226}Ra contributed negligibly to the total dose despite their occurrence in fish tissues, indicating limited transfer to edible tissues and lower radiological significance relative to ^{210}Pb and ^{210}Po. Similar findings have been reported in studies investigating radionuclide transfer in aquatic ecosystems, where dose contributions from uranium isotopes and radium are generally overshadowed by the more efficient bioaccumulation and radiological significance of ^{210}Pb and ^{210}Po (Anderson et al., 2014; Carvalho, 2011; Uddin et al., 2023)

Consistent with drinking water pathway (section 3.5), the biological effectiveness of ionizing radiation varies with radiation type. In fish tissues, ^{210} Po is an alpha emitter, whereas ^{210} Pb is predominantly betta emitter. Despite the higher relative biological effectiveness of alpha radiation, ^{210}Pb counted for 75-96% of the total AED in all fish species examined. This apparent discrepancy underscore that the effective dose contribution of any radionuclide is governed not by radiation type alone, but by interplay between its measured activity concentration in tissue, the specific energy per decay, and the radionuclide specific ingestion dose coefficient (IAEA, 2014; ICRP, 2013).

The predominance of ^{210}Pb observed in the present study contrasts with findings from many marine environments, where ^{210}Po is typically reported as the principal contributor to ingestion dose owing to its high radiotoxicity, efficient bioaccumulation, and strong trophic transfer in aquatic food webs (Carvalho, 2011; Fowler, 2011; Uddin et al., 2017). This difference likely reflects contrasting geochemical conditions between marine and freshwater ecosystems. In marine food webs, ^{210}Po is known to undergo efficient biological uptake and trophic transfer, often resulting in greater accumulation in fish tissues than its parent radionuclide, ^{210}Pb, by orders of magnitude (Carvalho, 2011; Štrok and Smodiš, 2011a). In contrast, the tropical freshwater river system investigated in the present study is characterised by strong catchment influence, high sediment load, seasonal hydrological variability, and mining-related disturbance, factors that may favour the transport, retention, and bioavailability of particle-reactive ^{210}Pb. The strong association of ^{210}Pb with suspended particles, organic matter, and bottom sediments enhances its accumulation within freshwater food webs, particularly in systems receiving substantial terrestrial and mining inputs (Anderson et al., 2014)

A recent global review by Johansen et al. (2025) further confirms that naturally occurring radionuclides account for more than 99% of the total seafood ingestion dose worldwide, with ^{210}Po contributing approximately 84% and ^{210}Pb about 8% in marine settings. While the relative contribution of ^{210}Pb in the present study (75% - 96%) is substantially higher than this global marine average, it is consistent with observations from other freshwater and mining-impacted environments, where sediment-associated ^{210}Pb dominates the radiological burden (Anderson et al., 2014; Štrok and Smodiš, 2011a). This finding underscores the importance of site-specific assessments, as the fractional contribution of individual radionuclides can deviate markedly from global averages depending on local geochemical conditions, catchment characteristics, and the nature of anthropogenic disturbance.

4. Conclusion and recomendations

This study provides an integrated assessment of radiological exposure from drinking water and freshwater fish consumption in a gold-mining-impacted region of Northern Tanzania. The results revealed pronounced source-, age-, species- and radionuclide-dependent variability in annual effective dose (AED) and excess lifetime cancer risk (ELCR), highlighting distinct exposure pathways and risk profiles associated with water and fish consumption.

Correlation analysis and PCA revealed that radionuclides distribution is largely governed by groundwater mineralisation and water-rock interaction. The strong association between uranium isotopes, EC, and TDS, particularly during the rainy season, suggests enhanced uranium transport through recharge pathways and weathered rock zones. In contrast, ^{226}Ra exhibited distinct geochemical behaviour indicating different mobilization mechanisms. The greatest variability observed in shallow wells compared with boreholes further highlights the sensitivity of shallow groundwater systems to hydrochemical changes.

Among the investigated water sources, shallow wells presented the greatest radiological concern, with AEDs exceeding WHO drinking water screening level of 0.1 mSv/y at several locations for all age groups However, across all age groups, children, particularly 5-year-olds, received the highest drinking water-derived doses, with AED at some sites approaching or exceeding the ICRP public dose reference level of 1 mSv/y, with uranium isotopes, especially ^{234}U, being the principal contributors to drinking water-derived doses. The consistently elevated ^{234}U/^{238}U activity ratios (>1) indicate uranium-series disequilibrium, attributed to alpha-recoil and radiation-induced lattice damage that enhance preferential mobilisation of ^{234}U in shallow aquifers. The estimated ELCR associated with drinking water ranged from 3.09×10^{-6} to 1.59×10^{-3} with elevated risks confined to a limited number of shallow wells locations characterised by higher radionuclide activity concentrations.

Fish consumption was identified as the principal pathway of radiological exposure, producing substantially higher doses and lifetime cancer risks than drinking-water ingestion. African lungfish consistently yielded the highest AEDs (1.06-3.61 mSv/y) and ELCR (4.99×10^{-3}), followed by tilapia (4.00×10^{-3}) and catfish (3.65×10^{-3}). Although infants received the highest annual doses owing to their greater radiological sensitivity, the lifetime cancer risks associated with consumption of all fish species exceeded the USEPA acceptable risk range (10^{-6}-10^{-4}), highlighting the need for continued radiological monitoring and risk mitigation in mining-impacted communities. Dose contributions were overwhelmingly dominated by ^{210}Pb and ^{210}Po while the combined contribution of ^{226}Ra, ^{238}U, ^{235}U, and ^{234}U was generally less than 1%, indicating that ^{210}Pb and ^{210}Po are the principal drivers of fish-derived radiological exposure.

Overall, while most drinking water sources posed relatively low radiological risk, several shallow wells exhibited elevated radionuclide concentrations and associated doses that warrant continued monitoring and site-specific assessment before use as drinking water sources. The elevated doses and cancer risks associated with fish consumption, particularly African lungfish, demonstrate that aquatic food pathways represent the dominant route of radionuclide exposure in the study area. These findings provide an important baseline for environmental monitoring and support the implementation of age-specific risk assessments and long-term surveillance programmes for radionuclides in both drinking water and aquatic food resources.

Limitations and future perspectives. This study is limited by temporal scope of sampling, assumptions used in the exposure assessment, and the absence of detailed hydrochemical data such as major ions, and alkalinity which would have improved interpretation of radionuclides behaviour. Geochemical speciation analyses were not performed, and this constrain mechanistic interpretation of radionuclides mobility and bioavailability. Future studies should therefore include expanded seasonal sampling, major ion chemistry, geochemical speciation modelling, and continued monitoring of the high-risk shallow wells and fish species to better constrain exposure patterns and improve radiological risk assessment in mining-impacted regions.

CRediT authorship contribution statement

Dorice Rashid Seif: Conceptualization, Data curation, Formal analysis, Methodology, Software, Visualization, Writing – original draft. **Leja Rovan Stiplošek:** Conceptualization, Methodology, Writing – review & editing. **Mwingereza John Kumwenda:** Formal analysis, Writing – review & editing. **Mohamed Mazunga:** Conceptualization, Methodology, Supervision, Writing – review & editing. **Marko Štrok:** Conceptualization, Data curation, Funding acquisition, Methodology, Supervision, Writing – review & editing.

Declaration of competing interest

The authors declare that they have no known competing financial interests or personal relationships that could have appeared to influence the work reported in this paper.

Acknowledgments

The authors acknowledge the financial and technical support provided by the International Atomic Energy Agency (IAEA) under Project IAEA INT0101, the Slovenian Research and Innovation Agency [programme P1 0143 and P2 0075], and Tanzania Commission of Science and Technology (COSTECH) through Muhimbili University of Health and Allied Sciences (MUHAS). They also extend their sincere thanks to the Department of Environmental Science at the Jožef Stefan Institute (IJS), Department of Physics, Department Geosciences and Department of Chemistry at the University of Dar es Salaam for their assistance and collaboration throughout this endeavour. Furthermore, the authors wish to acknowledge Dr. Watende Nyoni, Martin Kalinowski, Ivana Coha, Mugwe Thomas, and Elia Chacha for their numerous support, guidance and encouragement.

Appendix A. Supplementary data

Supplementary data to this article can be found online at https://doi.org/10.1016/j.jenvrad.2026.108119.

Data availability

Data will be made available on request.

References

Abed, M.F., Zarraq, G., Ahmed, S.H., 2021. Hydrogeochemical assessment of groundwater quality and its suitability for irrigation and domestic purposes in rural areas, north of baiji city-Iraq. Iraqi J. Sci. 2296–2306. https://doi.org/10.24996/ijs.2021.62.7.18.

Abou Zakhem, B., Al-Charideh, A., Kattaa, B., 2017. Using principal component analysis in the investigation of groundwater hydrochemistry of Upper Jezireh Basin, Syria. Hydrol. Sci. J. 62 (14), 2266–2279. https://doi.org/10.1080/02626667.2017.1364845.

Ademola, A.K., Bello, A.K., Adejumobi, A.C., 2014. Determination of natural radioactivity and hazard in soil samples in and around gold mining area in Itagunmodi, south-western, Nigeria. J. Radiat. Res. Appl. Sci. 7 (3), 249–255. https://doi.org/10.1016/j.jrras.2014.06.001.

Akoto, O., Gyimah, E., Zhan, Z., Xu, H., Nimako, C., 2020. Evaluation of health risks associated with trace metal exposure in water from the Barekese reservoir in Kumasi, Ghana. Hum. Ecol. Risk Assess. 26 (4), 1134–1148. https://doi.org/10.1080/10807039.2018.1559033.

Akpanowo, M.A., Bello, N.A., Umaru, I., Iyakwari, S., Joshua, E., Yusuf, S., Ekong, G.B., 2021. Assessment of radioactivity and heavy metals in water sources from artisanal mining areas of Anka, Northwest Nigeria. Sci. Afr. 12, e00761. https://doi.org/10.1016/j.sciaf.2021.e00761.

Al Hatmi, F., Embong, Z., Gismelseed, A., 2025. Assessment of radiological hazards due to natural radioactivity in groundwater from Al Masaraat aquifer, Oman. Phys. Chem. Earth, Parts A/B/C 140, 104012. https://doi.org/10.1016/j.pce.2025.104012.

Al-Masri, M.S., Mamish, S., Budeir, Y., Nashwati, A., 2000. 210Po and 210Pb concentrations in fish consumed in Syria. J. Environ. Radioact. 49 (3), 345–352. https://doi.org/10.1016/S0265-931X(99)00124-1.

Anderson, P., Barnett, C., Beresford, N., Bollhöfer, A., Bradshaw, C., Brittain, J., Brown, J.E., Choi, Y., Copplestone, D., Dagher, E., Dale, P., Doering, C., Dragovic, S., Ernst, P., Fesenko, E., Gashchak, S., Higley, K., Hosseini, A., Yankovich, T., 2014. HANDBOOK OF PARAMETER VALUES FOR THE PREDICTION OF RADIONUCLIDE TRANSFER TO WILDLIFE. *Technical Report Series no. 479*.

Baják, P., Csondor, K., Pedretti, D., Muniruzzaman, M., Surbeck, H., Izsák, B., Vargha, M., Horváth, Á., Pándics, T., Erőss, A., 2022. Refining the conceptual model for radionuclide mobility in groundwater in the vicinity of a Hungarian granitic complex using geochemical modeling. Appl. Geochem. 137, 105201. https://doi.org/10.1016/j.apgeochem.2022.105201.

Baják, P., Molnár, B., Hegedűs-Csondor, K., Tiljander, M., Jobbágy, V., Kohuth-Ötvös, V., Izsák, B., Vargha, M., Horváth, Á., Csipa, E., Óvári, M., Tóbi, C., Völgyesi, P., Pelczar, K., Hult, M., Erőss, A., 2023. Natural Radioactivity in Drinking Water in the Surroundings of a Metamorphic Outcrop in Hungary: the Hydrogeological Answer to Practical Problems. https://www.mdpi.com/2073-4441/15/9/1637.

Becher, J., Englisch, C., Griebler, C., Bayer, P., 2022. Groundwater fauna downtown – drivers, impacts and implications for subsurface ecosystems in urban areas. J. Contam. Hydrol. 248, 104021. https://doi.org/10.1016/j.jconhyd.2022.104021.

Bello, S., Nasiru, R., Garba, N.N., Adeyemo, D.J., 2020. Annual effective dose associated with radon, gross alpha and gross beta radioactivity in drinking water from gold mining areas of Shanono and Bagwai, Kano state, Nigeria. Microchem. J. 154, 104551. https://doi.org/10.1016/j.microc.2019.104551.

Benedik, L., Repinc, U., Štrok, M., 2010. Evaluation of procedures for determination of Ra-226 in water by α-particle spectrometry with emphasis on the recovery. Appl. Radiat. Isot. 68 (7–8), 1221–1225. https://doi.org/10.1016/j.apradiso.2009.12.005.

Benedik, L., Rovan, L., Falnoga, I., Jeran, Z., Lipej, L., Prosen, H., Faganeli, J., 2024. Po-210 in plankton and fish from coastal waters (gulf of Trieste, northern Adriatic Sea). Mar. Chem. 265–266, 104425. https://doi.org/10.1016/j.marchem.2024.104425.

Benedik, L., Rovan, L., Klemenčič, H., Gantar, I., Prosen, H., 2015. Natural radioactivity in tap waters from the private wells in the surroundings of the former Žirovski Vrh uranium mine and the age-dependent dose assessment. Environ. Sci. Pollut. Control Ser. 22 (16), 12062–12072. https://doi.org/10.1007/s11356-015-4481-z.

Boryło, A., Skwarzec, B., 2014. Activity disequilibrium between 234U and 238U isotopes in natural environment. J. Radioanal. Nucl. Chem. 300 (2), 719–727. https://doi.org/10.1007/s10967-014-3001-9.

Botwe, B.O., Schirone, A., Delbono, I., Barsanti, M., Delfanti, R., Kelderman, P., Nyarko, E., Lens, P.N.L., 2017. Radioactivity concentrations and their radiological significance in sediments of the Tema Harbour (Greater Accra, Ghana). J. Radiat. Res. Appl. Sci. 10 (1), 63–71. https://doi.org/10.1016/j.jrras.2016.12.002.

Carvalho, F.P., 2011. Polonium (210Po) and lead (210Pb) in marine organisms and their transfer in marine food chains. Journal of Environmental Radioactivity, International Topical Meeting on Polonium and Radioactive Lead Isotopes 102 (5), 462–472. https://doi.org/10.1016/j.jenvrad.2010.10.011.

Chander, S., Paikaray, S., Bansal, S., Sharma, K., Dhiman, D., Deshpande, R.D., 2023. δ18O and δ2H isotopes, trace metals and major ions in groundwater around uranium and fluoride contaminated Indus valley Quaternary alluvial plain, SW Punjab, India: implications on hydrogeochemical processes, irrigation use and source. Appl. Geochem. 152, 105652. https://doi.org/10.1016/j.apgeochem.2023.105652.

Cho, B.W., Choo, C.O., 2019. Geochemical behavior of uranium and radon in groundwater of Jurassic granite area, Icheon, Middle Korea. Water 11 (6), 1278. https://doi.org/10.3390/w11061278.

Choi, G., Kuiper, J.R., Bennett, D.H., Barrett, E.S., Bastain, T.M., Breton, C.V., Chinthakindi, S., Dunlop, A.L., Farzan, S.F., Herbstman, J.B., Karagas, M.R., Marsit, C.J., Meeker, J.D., Morello-Frosch, R., O'Connor, T.G., Pellizzari, E.D., Romano, M.E., Sathyanarayana, S., Schantz, S., et al., 2022. Exposure to melamine and its derivatives and aromatic amines among pregnant women in the United

States: the ECHO Program. Chemosphere 307, 135599. https://doi.org/10.1016/j.chemosphere.2022.135599.
Donaher, S.E., Dunn, R.P., Gonzales, A.K., Wattier, B.D., Powell, B.A., Martinez, N.E., 2023. Tissue-Specific toxicokinetics of aqueous Radium-226 in an estuarine mussel, Geukensia demissa. Environ. Sci. Technol. 57 (8), 3187–3197. https://doi.org/10.1021/acs.est.2c09421.
El-Taher, A., Alshahri, F., Elsaman, R., 2018. Environmental impacts of heavy metals, rare earth elements and natural radionuclides in marine sediment from Ras Tanura, Saudi Arabia along the Arabian Gulf. Appl. Radiat. Isot. 132, 95–104. https://doi.org/10.1016/j.apradiso.2017.11.022.
Farcas, A., Powell, C.F., Brookes, K.L., Merchant, N.D., 2020. Validated shipping noise maps of the Northeast Atlantic. Sci. Total Environ. 735, 139509. https://doi.org/10.1016/j.scitotenv.2020.139509.
Fasae, K.P., Isinkaye, M.O., 2018. Radiological risks assessment of 238U, 232Th and 40K in fish feeds and catfish samples from selected fish farms in Ado – ekiti, Nigeria. J. Radiat. Res. Appl. Sci. 11 (4), 317–322. https://doi.org/10.1016/j.jrras.2018.05.002.
Focus, E., Jackson, M., Simon, C., Njale, E., Kanyanemu, A., Siyajali Anatory, Y., Mhozya, M., Semiono, P., 2022. Risk assessment of natural radionuclides and radon gas in the artisanal and small-scale gold mine of buhemba, Tanzania. Int. J. Environ. Protect. Pol. 10 (3), 48. https://doi.org/10.11648/j.ijepp.20221003.12.
Fowler, S.W., 2011. 210Po in the marine environment with emphasis on its behaviour within the biosphere. Journal of Environmental Radioactivity, International Topical Meeting on Polonium and Radioactive Lead Isotopes 102 (5), 448–461. https://doi.org/10.1016/j.jenvrad.2010.10.008.
Friday, G.P., Cummins, C.L., Schwartzman, A.L., 1996. Radiological Bioconcentration Factors for Aquatic, Terrestrial, and Wetland Ecosystems at the Savannah River Site, p. 72.
Gartner, S.M., Whitlow, K.R., Laurence-Chasen, J.D., Kaczmarek, E.B., Granatosky, M.C., Ross, C.F., Westneat, M.W., 2022. Suction feeding of West African lungfish (Protopterus annectens): an XROMM analysis of jaw mechanics, cranial kinesis, and hyoid mobility. Biology Open 11 (9), bio059447. https://doi.org/10.1242/bio.059447.
Goulet, R.R., Newsome, L., Vandenhove, H., Keum, D.-K., Horyna, J., Kamboj, S., Brown, J., Johansen, M.P., Twining, J., Wood, M.D., Černe, M., Beaugelin-Seiller, K., Beresford, N.A., 2022. Best practices for predictions of radionuclide activity concentrations and total absorbed dose rates to freshwater organisms exposed to uranium mining/milling. J. Environ. Radioact. 244–245, 106826. https://doi.org/10.1016/j.jenvrad.2022.106826.
He, R., Liaw, S., Zhou, M., Zhou, X.-D., Luo, H., 2022a. Environmental evaluation of radioactivity levels and associated radiation hazards in groundwater around the WIPP site. Ecotoxicol. Environ. Saf. 242, 113849. https://doi.org/10.1016/j.ecoenv.2022.113849.
He, R., Liaw, S., Zhou, M., Zhou, X.-D., Luo, H., 2022b. Environmental evaluation of radioactivity levels and associated radiation hazards in groundwater around the WIPP site. Ecotoxicol. Environ. Saf. 242, 113849. https://doi.org/10.1016/j.ecoenv.2022.113849.
Hosseini, A., Thørring, H., Brown, J.E., Saxén, R., Ilus, E., 2008. Transfer of radionuclides in aquatic ecosystems – default concentration ratios for aquatic biota in the Erica tool. J. Environ. Radioact. 99 (9), 1408–1429. https://doi.org/10.1016/j.jenvrad.2008.01.012.
IAEA, 2010. Handbook of Parameter Values for the Prediction of Radionuclide Transfer in Terrestrial and Freshwater Environments. IAEA. https://www.iaea.org/publications/8201/handbook-of-parameter-values-for-the-prediction-of-radionuclide-transfer-in-terrestrial-and-freshwater-environments.
IAEA, 2014. Radiation Protection and Safety of Radiation Sources: *International Basic Safety Standards*. https://www.iaea.org/publications/8930/radiation-protection-and-safety-of-radiation-sources-international-basic-safety-standards.
ICRP, 2007a. The 2007 recommendations of the international commission on radiological protection. ICRP Publication 103. Ann. ICRP 37 (2–4). https://www.icrp.org/publication.asp?id=ICRP%20Publication%20103.
ICRP, 2007b. The 2007 Recommendations of the international commission on radiological protection. ICRP publication 103. Ann. ICRP 37 (2–4). Bing. https://www.bing.com/search?q=ICRP+Publication+103+(ICRP%2C+2007)&PC=U316&FORM=CHROMN.
ICRP, 2013. ICRP publication 119: compendium of dose coefficients based on ICRP publication 60.ICRP publication 119. Ann. ICRP 42 (4), 1–130. https://doi.org/10.1016/j.icrp.2013.05.003.
International Organization for Standardization (ISO), 2025. Determination of the Characteristic Limits (Decision Threshold, Detection Limit and Limits of the Coverage Interval) for Measurements of Ionizing radiation—Fundamentals and application—Part 1: Elementary Applications. International Organization for Standardization. ISO. https://www.iso.org/standard/90839.html.
Isinkaye, M.O., Fasanmi, P.O., Khandaker, M.U., Sayyed, M.I., Hanfi, M.Y., 2025. Assessment of elevated levels of natural radioactivity in groundwater of artisanal gold and gemstone mining sites and estimation of concomitant risk using monte carlo simulation approach. Radiat. Phys. Chem. 235, 112823. https://doi.org/10.1016/j.radphyschem.2025.112823.
Jakóbczyk-Karpierz, S., Ślósarczyk, K., Sitek, S., 2020. Tracing multiple sources of groundwater pollution in a complex carbonate aquifer (Tarnowskie Góry, southern Poland) using hydrogeochemical tracers, TCE, PCE, SF6 and CFCs. Appl. Geochem. 118, 104623. https://doi.org/10.1016/j.apgeochem.2020.104623.
Jeffree, R.A., Simpson, R.D., 1986. An experimental study of the uptake and loss of Ra-226 by the tissue of the tropical freshwater musselVelesunio angasi (Sowerby) under varying Ca and Mg water concentrations. Hydrobiologia 139 (1), 59–80. https://doi.org/10.1007/BF00770242.
Jeffree, R.A., Simpsonf, R.D., 1984. Radium-226 is accumulated in calcium granules in the tissues of the freshwater mussel, *velesunio angasi*: support for a metabolic analogue hypothesis? Comp. Biochem. Physiol. Physiol. 79 (1), 61–72. https://doi.org/10.1016/0300-9629(84)90708-4.
Jia, G., Belli, M., Blasi, M., Marchetti, A., Rosamilia, S., Sansone, U., 2001. Determination of 210Pb and 210Po in mineral and biological environmental samples. J. Radioanal. Nucl. Chem. 247 (3), 491–499. https://doi.org/10.1023/A:1010605804815.
Johansen, M.P., Gwynn, J.P., Carpenter, J.G., Charmasson, S., Mori, A., Orr, B., Simon-Cornu, M., Osvath, I., Mc Ginnity, P., 2025. Which radionuclides contribute most to seafood ingestion dose? J. Environ. Radioact. 287, 107706. https://doi.org/10.1016/j.jenvrad.2025.107706.
Kabete, J.M., Groves, D.I., McNaughton, N.J., Mruma, A.H., 2012. A new tectonic and temporal framework for the Tanzanian Shield: implications for gold metallogeny and undiscovered endowment. Ore Geol. Rev. 48, 88–124. https://doi.org/10.1016/j.oregeorev.2012.02.009.
Kaur Guron, B., Kalkal, S., Mehra, R., 2025. The impact of uranium contamination in groundwater on human health: a toxicological risk assessment. Int. J. Environ. Anal. Chem. 105 (13), 3058–3072. https://doi.org/10.1080/03067319.2024.2337883.
Kazimoto, E.O., Ikingura, J.R., 2014. Trace element geochemistry and petrogenesis of the granitoids and high-K andesite hosting gold mineralisation in the Archean Musoma-Mara Greenstone Belt, Tanzania. J. Afr. Earth Sci. 91, 66–78. https://doi.org/10.1016/j.jafrearsci.2013.12.003.
Kazoka, A.R., Mwalilino, J., Mtoni, P., 2023. A radiological risk assessment of 226Ra, 228Ra and 40K isotopes in tilapia fish and its granitic environment in Singida municipality, Tanzania. Earth 4 (3), 540–551. https://doi.org/10.3390/earth4030028.
Kihampa, C., Wenaty, A., 2013. Impact of mining and farming activities on water and sediment quality of the Mara river basin, Tanzania. Research Journal of Chemical Sciences ISSN 2231, 606X.
Kimaro, E., Mohammed, N., 2015. Natural radioactivity levels in the area around the uranium deposit of the bahi district in Dodoma Region, Tanzania. Int. Res. J. Pure Appl. Chem. 9 (3), 1–10. https://doi.org/10.9734/IRJPAC/2015/17747.
Kumar, A., Karpe, R.K., Rout, S., Gautam, Y.P., Mishra, M.K., Ravi, P.M., Tripathi, R.M., 2016. Activity ratios of 234 U/238 U and 226 Ra/228 Ra for transport mechanisms of elevated uranium in alluvial aquifers of groundwater in south-western (SW) Punjab, India. J. Environ. Radioact. 151, 311–320. https://doi.org/10.1016/j.jenvrad.2015.10.020.
Kumar, A., Tripathi, R.M., Rout, S., Mishra, M.K., Ravi, P.M., Ghosh, A.K., 2014. Characterization of groundwater composition in Punjab state with special emphasis on uranium content, speciation and mobility. Radiochim. Acta 102 (3), 239–254. https://doi.org/10.1515/ract-2014-2109.
Lacroix-Durand, C., Janz, D., Liber, K., 2025. Chronic Radium-226 toxicity to and oxidative stress in the aquatic invertebrate Chironomus dilutus. Toxicol. Res. 14 (1), tfaf001. https://doi.org/10.1093/toxres/tfaf001.
Lapworth, D.J., Nkhuwa, D.C.W., Okotto-Okotto, J., Pedley, S., Stuart, M.E., Tijani, M.N., Wright, J., 2017. Urban groundwater quality in Sub-Saharan Africa: current status and implications for water security and public health. Hydrogeol. J. 25 (4), 1093–1116. https://doi.org/10.1007/s10040-016-1516-6.
Li, J., Li, Z., Brandis, K.J., Bu, J., Sun, Z., Yu, Q., Ramp, D., 2020. Tracing geochemical pollutants in stream water and soil from mining activity in an alpine catchment. Chemosphere 242, 125167. https://doi.org/10.1016/j.chemosphere.2019.125167.
Ligate, F., Lucca, E., Ijumulana, J., Irunde, R., Kimambo, V., Mtamba, J., Ahmad, A., Hamisi, R., Maity, J.P., Mtalo, F., Bhattacharya, P., 2022. Geogenic contaminants and groundwater quality around Lake Victoria goldfields in northwestern Tanzania. Chemosphere 307, 135732. https://doi.org/10.1016/j.chemosphere.2022.135732.
Martin, S.M.W., Philip, O.O., Fredrick, O.K., Ayub, V.O.O., Said-Ally, M., 2018. Influence of land use practices on water physicochemical parameters and nutrients loading along the Mara River of East Africa. Afr. J. Environ. Sci. Technol. 12 (7), 235–243. https://doi.org/10.5897/AJEST2015.2021.
Matiatos, I., Alexopoulos, A., Godelitsas, A., 2014. Multivariate statistical analysis of the hydrogeochemical and isotopic composition of the groundwater resources in northeastern Peloponnesus (Greece). Sci. Total Environ. 476–477, 577–590. https://doi.org/10.1016/j.scitotenv.2014.01.042.
Mourad, S., Ayoub, G.M., Al Hindi, M., Zayyat, R.M., 2021. Occurrence and hazard assessment of natural radioactivity in drinking water in South Lebanon. Environ. Monit. Assess. 193 (6), 358. https://doi.org/10.1007/s10661-021-09133-8.
Mshiu, E., Maboko, Makenya A.H., Maboko, Makenya A.H., 2008. Aerogeophysical, geological and geochemical investigation of the late Archaean granitoids in the Musoma- Mara greenstone Belt, NE Tanzania. https://www.academia.edu/75498848/Aerogeophysical_Geological_and_Geochemical_Investigation_of_the_Late_Archaean_Granitoids_in_the_Musoma_Mara_Greenstone_Belt_NE_Tanzania.
Nkinda, M.S., Rwiza, M.J., Ijumba, J.N., Njau, K.N., 2021. Heavy metals risk assessment of water and sediments collected from selected river tributaries of the Mara River in Tanzania. Discover Water 1 (1), 3. https://doi.org/10.1007/s43832-021-00003-5.
Nteziyaremye, P., Omara, T., 2020. Bioaccumulation of priority trace metals in edible muscles of West African lungfish (Protopterus annectens Owen, 1839) from Nyabarongo River, Rwanda. Cogent Environ. Sci. 6 (1), 1779557. https://doi.org/10.1080/23311843.2020.1779557.
Nuccetelli, Rusconi, R., Forte, M., 2012b. Radioactivity in drinking water: regulations, monitoring results and radiation protection issues. https://www.researchgate.net/publication/233940881_Radioactivity_in_drinking_water_Regulations_monitoring_results_and_radiation_protection_issues.
Nuccetelli, C., Rusconi, R., Forte, M., 2012a. Radioactivity in drinking water: regulations, monitoring results and radiation protection issues. Annali Dell'Istituto Superiore Di Sanità 48, 362–373.

Nursapina, N.A., Shynybek, B.A., Matveyeva, I.V., Nazarkulova, Sh N., Štrok, M., Benedik, L., Ponomarenko, O.I., 2022. Effect of mineral fertilisers application on the transfer of natural radionuclides from soil to radish (Raphanus sativus L.). J. Environ. Radioact. 247, 106863. https://doi.org/10.1016/j.jenvrad.2022.106863.
Omolo, D., Langat, P.K., Koech, R., Jiang, Y., 2018. Living off wetlands: a case Study of Mara Bay and masirori wetlands, Tanzania. J. Geosci. Environ. Protect. 6 (12), 43–60. https://doi.org/10.4236/gep.2018.612003.
Banzi, F.P., 2016a. Natural radioactivity in water and its potential human health risk in the vicinity of Mkuju River uranium Project in Tanzania. Int. J. Environ. Protect. Pol. 4 (5), 111. https://doi.org/10.11648/j.ijepp.20160405.11.
Banzi, F.P., 2016b. Natural radioactivity in water and its potential human health risk in the vicinity of Mkuju River uranium Project in Tanzania. Int. J. Environ. Protect. Pol. 4 (5), 111. https://doi.org/10.11648/j.ijepp.20160405.11.
Planinšek, P., Smodiš, B., Benedik, L., 2016. Simultaneous determination and uptake assessment of selected radionuclides in plants grown in substrate contaminated with U-mill tailings. J. Radioanal. Nucl. Chem. 309 (1), 351–365. https://doi.org/10.1007/s10967-016-4881-7.
Putri, S., Putra, D., Pambudi, F., Makmur, M., Prihatiningsih, W., Yusuf, S., rina mulyaningsih, T., 2022. Analysis of polonium-210 and dose assessment in marine fishery muscle from Southern Coast of Sukabumi. IOP Conf. Ser. Earth Environ. Sci. 1119, 012085. https://doi.org/10.1088/1755-1315/1119/1/012085.
Rožmarić, M., Rogić, M., Benedik, L., Štrok, M., 2012a. Natural radionuclides in bottled drinking waters produced in Croatia and their contribution to radiation dose. Sci. Total Environ. 437, 53–60. https://doi.org/10.1016/j.scitotenv.2012.07.018.
Rožmarić, M., Rogić, M., Benedik, L., Štrok, M., Barišić, D., Gojmerac Ivšić, A., 2012b. 210Po and 210Pb activity concentrations in Mytilus galloprovincialis from Croatian Adriatic coast with the related dose assessment to the coastal population. Chemosphere 87 (11), 1295–1300. https://doi.org/10.1016/j.chemosphere.2012.01.039.
Rovan, L., Zuliani, T., Horvat, B., Kanduč, T., Vreča, P., Jamil, Q., Čermelj, B., Bura-Nakić, E., Cukrov, N., Štrok, M., Lojen, S., 2021. Uranium isotopes as a possible tracer of terrestrial authigenic carbonate. Sci. Total Environ. 797, 149103. https://doi.org/10.1016/j.scitotenv.2021.149103.
Smodiš, B., Štrok, M., Černe, M., 2014. Radioecology around a closed uranium mine. J. Radioanal. Nucl. Chem. 299 (1), 765–771. https://doi.org/10.1007/s10967-013-2697-2.
Srivastava, S.K., Balbudhe, A.Y., Vishwa Prasad, K., Padma Savithri, P., Tripathi, R.M., Puranik, V.D., 2013. Variation in the uranium isotopic ratios ^{234}U/^{238}U, ^{238}U/total-U and ^{234}U/total-U in Indian soil samples: application to environmental monitoring. Radioprotection 48 (2), 231–242. https://doi.org/10.1051/radiopro/2012044.
Stabile, L., Buonanno, G., Ficco, G., Scungio, M., 2017. Smokers' lung cancer risk related to the cigarette-generated mainstream particles. J. Aerosol Sci. https://doi.org/10.1016/j.jaerosci.2017.02.005.
Sunday, J.S., Sowunmi, A.A., Akomolafe, I.R., Jibiri, N.N., 2025. Evaluation of radiological risks from radionuclides in fish and sediment of Eleyele Reservoir, Ibadan, Nigeria. Environ. Health Insights 19, 11786302251347017. https://doi.org/10.1177/11786302251347017.
Tanasković, I., Golobocanin, D., Miljević, N., 2012. Multivariate statistical analysis of hydrochemical and radiological data of Serbian spa waters. J. Geochem. Explor. 112, 226–234. https://doi.org/10.1016/j.gexplo.2011.08.014.
Temesgen, M., Getahun, A., Lemma, B., Janssens, G.P.J., 2022. Food and feeding biology of Nile Tilapia (Oreochromis niloticus) in Lake Langeno, Ethiopia. Sustainability 14 (2), 974. https://doi.org/10.3390/su14020974.
Tesfahun, A., Alebachew, S., 2023. Diet composition and feeding habits of the African sharptooth catfish Clarias gariepinus (Burchell, 1822) from Ribb Reservoir, South Gondar, Ethiopia. Cogent Food Agric. 9 (2), 2284228. https://doi.org/10.1080/23311932.2023.2284228.
Tonev, D., Geleva, E., Slavchev, B., Dobrev, L., Protohristov, H., Veleva, B., Goutev, N., Demerdjiev, A., Dimitrova, D., Nikolova, N., 2023. Investigation of natural radioactivity in drinking water sources in South-Central Bulgaria. J. Radioanal. Nucl. Chem. 332 (11), 4641–4649. https://doi.org/10.1007/s10967-023-08983-5.
Štrok, M., Repinc, U., Smodiš, B., 2008. Calibration and validation of a proportional counter for determining beta emitters. Journal of Power and Energy Systems 2 (2), 573–581. https://doi.org/10.1299/jpes.2.573.
Štrok, M., Smodiš, B., Petrinec, B., 2010a. Natural radionuclides in sediments and rocks from Adriatic Sea. J. Radioanal. Nucl. Chem. 286 (2), 303–308. https://doi.org/10.1007/s10967-010-0705-3.
Štrok, M., Smodiš, B., Petrinec, B., 2010b. Natural radionuclides in sediments and rocks from Adriatic Sea. J. Radioanal. Nucl. Chem. 286 (2), 303–308. https://doi.org/10.1007/s10967-010-0705-3.
Štrok, M., Smodiš, B., Petrinec, B., 2010c. Natural radionuclides in sediments and rocks from Adriatic Sea. J. Radioanal. Nucl. Chem. 286 (2), 303–308. https://doi.org/10.1007/s10967-010-0705-3.
Štrok, M., Smodiš, B., 2011a. Levels of 210Po and 210Pb in fish and molluscs in Slovenia and the related dose assessment to the population. Chemosphere 82 (7), 970–976. https://doi.org/10.1016/j.chemosphere.2010.10.075.
Štrok, M., Smodiš, B., 2011b. Levels of 210Po and 210Pb in fish and molluscs in Slovenia and the related dose assessment to the population. Chemosphere 82 (7), 970–976. https://doi.org/10.1016/j.chemosphere.2010.10.075.
Štrok, M., Smodiš, B., 2011c. Natural radionuclides in milk from the vicinity of a former uranium mine. Nucl. Eng. Des. 241 (4), 1277–1281. https://doi.org/10.1016/j.nucengdes.2010.03.035.
Štrok, M., Smodiš, B., 2011d. Natural radionuclides in milk from the vicinity of a former uranium mine. Nucl. Eng. Des. 241 (4), 1277–1281. https://doi.org/10.1016/j.nucengdes.2010.03.035.
Uddin, S., Fowler, S.W., Behbehani, M., 2023. 210Po in the environment: reassessment of dose to humans. Sustainability 15 (2), 1674. https://doi.org/10.3390/su15021674.
Uddin, S., Fowler, S.W., Behbehani, M., Metian, M., 2017. 210Po bioaccumulation and trophic transfer in marine food chains in the northern Arabian Gulf. Journal of Environmental Radioactivity, INCO-PoPb-2015 174, 23–29. https://doi.org/10.1016/j.jenvrad.2016.08.021.
Ugbede, F.O., Aduo, B.C., Ogbonna, O.N., Ekoh, O.C., 2020. Natural radionuclides, heavy metals and health risk assessment in surface water of Nkalagu river dam with statistical analysis. Sci. Afr. 8, e00439. https://doi.org/10.1016/j.sciaf.2020.e00439.
UNSCEAR, 2000. UNSCEAR report 2000: sources and effects of ionizing radiation. *United Nations Scientific Comittee on the Effects of Atomic Radiation—PubMed*. https://pubmed.ncbi.nlm.nih.gov/11281539/.
UNSCEAR, 2016. Source, effects, and Risks of Ionizing Radiation. United Nations : Scientific Committee on the Effects of Atomic Radiation. https://www.unscear.org/unscear/en/publications/1996.html.
U.S. EPA, 1989. *Risk Assessment Guidance for Superfund: Pt. A. Human Health Evaluation Manual*. Office of Emergency and Remedial Response. U.S. Environmental Protection Agency.
Uzorka, A., Tukahirwa, I., Ouyesiga, L., Olaniyan, A.O., 2025. Analysis of radionuclide concentrations in fish and radioactivity levels in water from Lake Edward, Rukungiri District, Uganda. Discov. Environ. 3 (1), 71. https://doi.org/10.1007/s44274-025-00266-y.
Vengosh, A., Coyte, R.M., Podgorski, J., Johnson, T.M., 2022. A critical review on the occurrence and distribution of the uranium- and thorium-decay nuclides and their effect on the quality of groundwater. Sci. Total Environ. 808, 151914. https://doi.org/10.1016/j.scitotenv.2021.151914.
Viloria, T., Pesantez, A., Vázquez Silva, E., Delgado, M., Duque-Sarango, P., Sajó-Bohus, L., 2020. Levels of radium-226 in the rainbow trout, macroinvertebrates-substrates and water adjacent to the mining concession Loma Larga, Azuay-Ecuador. Earth Sci. Res. J. 24, 29–34. https://doi.org/10.15446/esrj.v24n1.79728.
VPO, 2022. Mara River Pollution Report.
Vrecek, P., Benedik, L., Pihlar, B., 2004. Determination of 210Pb and 210Po in sediment and soil leachates and in biological materials using a Sr-resin column and evaluation of column reuse. Appl. Radiat. Isot.: Including Data, Instrumentation and Methods for Use in Agriculture, Industry and Medicine 60 (5), 717–723. https://doi.org/10.1016/j.apradiso.2003.11.088.
World Health Organization, 2011. Guidelines for drinking-water Quality.
World Health Organization, 2022a. Guidelines for drinking-water Quality: Incorporating the First and Second Addenda. World Health Organization.
World Health Organization (WHO), 2022b. Guidelines for drinking-water Quality.
Wu, Y., Li, J., Wang, Y., Xie, X., 2018. Variations of uranium concentrations in a multi-aquifer system under the impact of surface water-groundwater interaction. J. Contam. Hydrol. 211, 65–76. https://doi.org/10.1016/j.jconhyd.2018.03.007.
Zhang, Z., Yi, L., Ren, H., Lyu, T., Liu, C., Li, S., Bian, H., Wang, C., Ren, L., Liu, N., Wang, H., Dong, Y., Li, R., 2025. Geochemical behavior of high-level radium contamination in representative coastal saltworks. J. Hydrol. 652, 132716. https://doi.org/10.1016/j.jhydrol.2025.132716.